

---

# Calibration measurements of a Microwave Discharge Hydrogen Lamp

BACHELOR RESEARCH PROJECT

---

*Author:*  
M.L. BOTH

*Student number:*  
11036877

*Coaches:*  
L.H. ARNTZEN  
M.C. VLOEMANS

*Supervisors:*  
N.F.W. LIGTERINK, MSc  
Prof. Dr. H.V.J. LINNARTZ

**THE HAGUE**  
UNIVERSITY OF  
APPLIED SCIENCES

June 4, 2015

Sackler Laboratory for Astrophysics



## Abstract

In the Sackler Laboratory for Astrophysics interstellar ices on dust grains are simulated and different processes are characterized quantitatively to get a better understanding of the evolutionary stages and chemistry of star formation. One of the processes that has been studied is the interaction between the ices and vacuum ultraviolet (VUV) radiation that is largely dominating the interstellar radiation field. Such light is generated by a Microwave Discharge Hydrogen Lamp, and for quantitative applications the system has to be calibrated. This calibration concerns the full spectral emission pattern, i.e., flux as function of emitted wavelength. For this a VUV spectrometer is used.

Absolute photon fluxes are determined with O<sub>2</sub>-actinometry for three different lamp settings and typically are of the order of 10<sup>13</sup> photons s<sup>-1</sup> cm<sup>-2</sup>. A comparison with the determined fluxes in Ligterink et al. (2015 in prep.) for the same settings, shows that the wavelength dependence of O<sub>2</sub>-actinometry has a substantial effect on the measured flux. For a lamp emission pattern with more Lyman- $\alpha$  (121 nm) flux than molecular (~160 nm), the measured flux with O<sub>2</sub>-actinometry will give a lower value than in the reverse case. O<sub>2</sub>-actinometry, therefore, is not a good way to measure the absolute photon flux, but nevertheless a good method to get an idea of the flux's order of magnitude during the photodesorption, photodestruction and photochemistry experiments.

The goal of this research project has been to systematically investigate the emission pattern of the used lamp in full dependence of a number of experimental settings. These are discussed. Moreover, a number of practical issues, such as window degradation, were noticed and are described as well.



# Contents

<b>1</b>	<b>Introduction</b>	<b>1</b>
<b>2</b>	<b>Theory</b>	<b>3</b>
2.1	Astrochemistry . . . . .	3
2.1.1	Grains . . . . .	4
2.2	UV radiation . . . . .	5
2.3	O <sub>2</sub> -actinometry . . . . .	6
<b>3</b>	<b>Experimental</b>	<b>9</b>
3.1	Detection techniques . . . . .	9
3.2	VUV spectrometer . . . . .	11
3.3	UV lamp . . . . .	11
3.4	Samples . . . . .	12
3.4.1	Background deposition . . . . .	12
3.4.2	Direct deposition . . . . .	13
<b>4</b>	<b>Results</b>	<b>15</b>
4.1	Measured VUV spectra . . . . .	15
4.2	O <sub>2</sub> -actinometry measurements . . . . .	20
4.3	UV/VIS spectrometer . . . . .	23
4.3.1	Color fluctuations . . . . .	26
<b>5</b>	<b>Conclusion</b>	<b>29</b>
	<b>Acknowledgements</b>	<b>31</b>
	<b>Bibliography</b>	<b>33</b>
<b>A</b>	<b>Fluxes of other O<sub>2</sub>-actinometry measurements</b>	<b>35</b>
<b>B</b>	<b>Position sample</b>	<b>37</b>
<b>C</b>	<b>Originele omschrijving afstudeeropdracht</b>	<b>39</b>



# Chapter 1

## Introduction

The interstellar medium, the space between the stars, is not completely empty but filled with atoms and molecules in the gas and solid phase. Dark clouds are formed in the interstellar medium and have a higher density than the surrounding area. One of the processes in these clouds is the freeze out of gas particles on dust grains. The ices on the dust grains are studied to get a better understanding of the evolutionary stages and chemistry of star formation in the Milky Way (Herbst and van Dishoeck, 2009). Icy dust grains offer a molecule reservoir where solid state reactions take place. An external trigger is provided by Vacuum Ultraviolet (VUV) photons, arising from excited hydrogen or also from background stars. Impacting VUV photons may induce molecules to evaporate from the surface (photodesorption) or to dissociate, triggering reactions that may yield complex organic molecules (COMs, molecules with C–H bonds and more than 6 atoms). In the laboratory the ices on the dust grains are reproduced. Molecules are deposited on a  $\text{MgF}_2$  transmission window and can be measured by two different kind of analysis techniques. The vibrational absorption of the ice is measured with infrared spectroscopy and the released molecules and atoms can be measured by a quadrupole mass spectrometer. With these techniques the effect of ultraviolet light on ices such as photodesorption, photodestruction and photochemistry are studied.

In the set up that is used here the ultraviolet light is simulated with a Microwave Discharge Hydrogen Lamp (MDHL). This lamp is a glass tube filled with hydrogen gas. With the use of a microwave generator a plasma is generated in the lamp. The lamp has different settings: gas type, pressure, lamp type, pump speed and direction, position of the cavity and the input power of the microwave. Each of these parameters causes a different spectral energy distribution (SED) and an absolute photon flux. For the experiments it is important to know the photon density per second on the ice, therefore the lamps must be well calibrated.

In Ligterink et al. (2015 in prep.) research is done on the spectral energy distribution of the MDHL at different settings. The spectra are recorded by a calibrated VUV monochromator. Here, the absolute photon flux is measured in  $\mu\text{W } \lambda^{-1} \text{ sr}^{-1} \text{ mm}^{-2}$ . Using a NIST calibrated photodiode the flux in photons  $\lambda^{-1} \text{ s}^{-1} \text{ cm}^{-2}$  is determined. This is done for several settings of the lamp. Up to now a common way, for all the researches using a MDHL, to measure the flux is by  $\text{O}_2$ -actinometry. This technique makes use of the formation of ozone when VUV photons interact with oxygen ice. The formation of ozone can be detected with a infrared spectrometer. Through the known band strength of ozone the photon flux can be calculated. In this thesis  $\text{O}_2$ -actinometry is used to determine the photon flux at different settings of the lamp, and will be compared with the data of Ligterink et al. (2015 in prep.). In order to understand what is

actually measured with O<sub>2</sub>-actinometry.

Also, in the laboratory a new VUV spectrometer was recently installed on the set up. With this spectrometer the spectrum of the MDHL can be measured. By measuring different spectra the operation of the new spectrometer has been studied, with the use of the spectra from Ligterink et al. (2015 in prep.).

The MDHL has also a spectrum in the visible part of the electro magnetic spectrum. With a spectrometer for visible light the behavior and flux of a specific line in the ultraviolet range can be measured. With the flux of that specific line and the spectra from (Ligterink et al., 2015 in prep.) the absolute photon flux of ultraviolet range of the MDHL can be determined, using a spectrometer in the visible regime.

# Chapter 2

## Theory

In this chapter the basic principles of astrochemistry are discussed. This is important to get a better understanding of the main project. Also the theory of the ultraviolet radiation of hydrogen and the technique to calibrate the MDHL are explained.

### 2.1 Astrochemistry

Interstellar clouds are formed when the density of the matter increases due to gravity. Diffuse clouds, with a density of about  $n \sim 100 \text{ cm}^{-3}$  and a kinetic temperature around 100 K, change into dark clouds, which have densities of  $n \sim 10^4 - 10^8 \text{ cm}^{-3}$  and a kinetic temperature between 10-100 K (Herbst and van Dishoeck, 2009). Dark clouds can be light-years wide and because of the high density almost no optical light can pass through the clouds. Figure 2.1a shows that the dark cloud contains cores with a higher density than the surrounding area. The cores further collapse under their gravity and the star formation starts ( $t=0$ , figure 2.1b). All the matter in the envelope, the area around the cores, gets attracted and absorbed by the gravitational collapse which forms a protostar, and this takes about  $10^4 - 10^5$  years. A protostar is a high density mass object where nuclear fusion has not started yet. A disk of high density matter forms around the protostar. The protostar still absorbs the matter in the area and forms two bipolar outflows, see figure 2.1c. These outflows consist of radiation and gas with a high velocity and are formed because of the conservation of angular momentum. Depending on the strength of the shocks created by the outflows, the particles in the surrounding cloud can be destroyed. Because the temperature of the outflows is high it is possible to cause chemical reactions in the surrounding cloud. The protostar gets its energy by the collisions of the absorbed matter. When the temperature has raised enough to start nuclear fusion it becomes a young stellar object (YSO), see figure 2.1d. At that moment the YSO still absorbs the matter in the envelope and increases in mass. After about  $10^6 - 10^7$  years the star has absorbed all the matter, see figure 2.1e. The

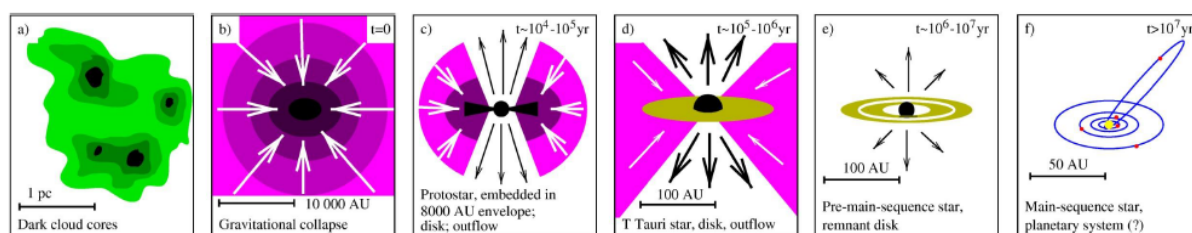


Figure 2.1: Evolutionary stages of star formation (Hogerheijde (1998), after Shu et al. (1987)).

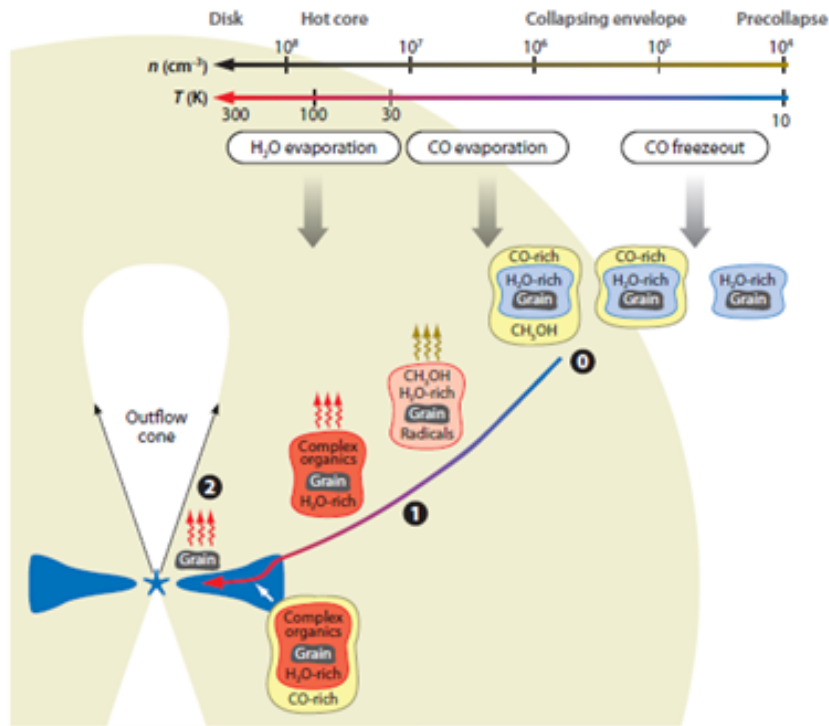


Figure 2.2: Evolution of the grain entering the protoplanetary disk. The temperature and density scale refers to the envelope, not the disk. (Herbst and van Dishoeck, 2009).

matter in the disk around the star forms lumps that stick together. In the end the lumps can form planets and a new star system is born, see figure 2.1f.

Because the dark clouds are big and have a high density the InterStellar Radiation Field (ISRF), generated by stars, cannot pass through the cloud. This results in the temperature going down in the center of the cloud. In the cloud are dust particles, dust grains, that can be found at different states of star formation. They are found in the dark cloud before it collapses under its gravity and in the inflow of the (proto)star.

### 2.1.1 Grains

The grains are made of silicate and carbonaceous material and have a size of  $\sim 0.01\text{-}0.5 \mu\text{m}$ . The temperature of the grains is about 10 K which causes the gas of the surrounding cloud to condense on the grain and form an ice layer. The accretion of the gas particles occurs by physical adsorption (weak van der Waals forces) because of the low temperatures. Different species will condense on the grain (except  $\text{H}/\text{H}_2$ ) as soon as their freeze-out temperature has been reached, which means that the ice can grow in different layers with different composition. In figure 2.2 an example is given of the ice layers on a grain in the envelope. In the outer envelope the temperature is low and the grain in the figure has already a layer of  $\text{H}_2\text{O}$ -rich ice. CO will freeze out on the  $\text{H}_2\text{O}$ -rich layer of ice and new molecules will be formed, like methanol. In the surrounding area of the (proto)star the temperature increases. By moving closer to the (proto)star the species will evaporate and leave the grain at different temperatures. The surface of the grain has different energy states. For particles the situation could be de-

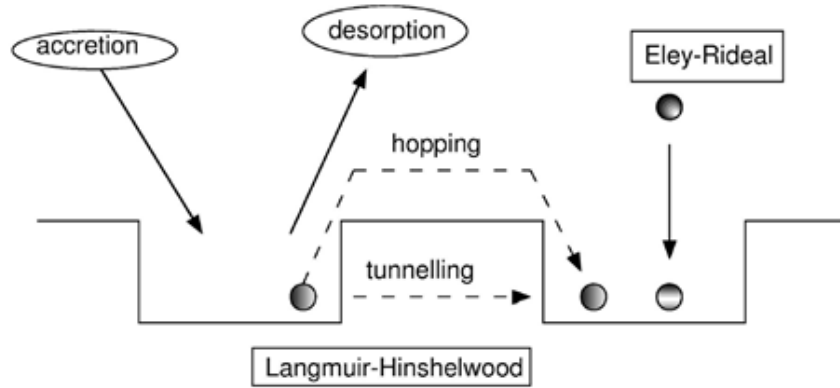


Figure 2.3: Grain surface reactions (Herbst and van Dishoeck, 2009).

scribed like they are captured in a finite potential well. To move to another well the particle needs a certain energy ( $E_B$ ) to hop over the energy barrier. The particle can also quantum tunnel through the barrier, mostly light atoms. When two particles encounter each other they can form a new molecule. The energy that is released by the formation can give the molecule enough energy to leave the grain, called desorption energy ( $E_D$ ). There are two mechanisms through which particles can react and release the grain: the diffuse mechanism (Langmuir-Hinshelwood) and direct mechanism (Eley-Rideal), see figure 2.3. The diffuse mechanism is when a particle first sticks on the surface, diffuse over the surface and then encounters another particle, possibly leading to the formation of a new molecule. The other mechanism is when a gas particle collides with another particle on the grain, the formation can take place directly. Grains thus form a place where atoms and molecules can react to form larger species.

## 2.2 UV radiation

The ISRF is composed of light from stars (and other stellar objects) and emission of photons by excited hydrogen atoms and molecules. Stars act as black body emitters, that is, the spectrum of the derived electromagnetic waves depends on their temperature. The emitted radiation has a continuous spectrum which also can have radiation in the ultraviolet range.

In the dark clouds a large amount of hydrogen is present. A hydrogen atom comprises one proton and one electron. Normally the electron is located in the state with the lowest energy, quantum number  $n=1$ . But when the atom gets external energy, for example by collisions with other atoms or cosmic rays or by absorption of a photon, the electron can move to a higher energy state,  $n>1$ . Finally the electron will decay to  $n=1$ , emitting a photon. Lyman- $\alpha$ , a photon produced by the decay of the electron from the  $n=2$  state to the  $n=1$  state, has an energy of 10.2 eV and a wavelength of 121.6 nm. Not only the Lyman- $\alpha$  photon gets emitted by the hydrogen atom, also the other possible decays will take place when the electron is excited to a higher state than  $n=2$ . In case of a hydrogen molecule the energy distribution changes from a line spectrum to a band spectrum. This is caused because it is now possible for the hydrogen to vibrate. The cumulative radiation of hydrogen in the interstellar medium is a combination between the spectrum of a hydrogen atom and a hydrogen molecule.

The frequency that ultraviolet photons impact on dust grains in the dense interstellar medium is around one per day per grain. When the photon hits the icy grain the energy of the photon can trigger different processes. When the photon hits an atom or molecule on the grain it can

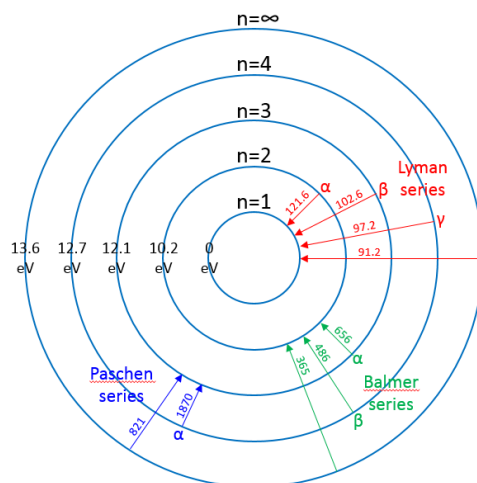


Figure 2.4: Schematic representation of a hydrogen atom with the transitions of the Lyman, Balmer and Paschen series.

transfer its energy. The excess energy may be high enough to allow the particle to evaporate from the surface, this is called photodesorption. It is also possible that the photon, when the energy is high enough, breaks a molecular bond in a molecule, called photodissociation. The molecule splits in different parts which are still stuck on the grain. The particles typically radical species, diffuse over the surface until they encounter another particle and form a new molecule, called photochemistry.

## 2.3 O<sub>2</sub>-actinometry

The total internal energy ( $E_{mol}$ ) of a molecule is made up by three different energies: Electronic energy ( $E_{el}$ ), vibrational energy ( $E_{vib}$ ) and rotational energy ( $E_{rot}$ ), see figure 2.5.

$$E_{mol} = E_{el} + E_{vib} + E_{rot} \quad (2.1)$$

Each molecule has its own specific set of transitions, governed by energy differences between electronic quantum states. That means that when an electron falls back to a lower energy shell it can emit a photon with one of the specific energies typical for that molecule. The energies between the different electronic states (n-states) are quite large and correspond with energies typical for UV light and visible light. Normally the electrons are located in the lowest energy states, but when they absorb external energy they can move to higher energy states. The atoms in a molecule have the ability to vibrate. At every electronic state there are several vibrational states (v-states) possible. It takes less energy to excite a molecular vibration and this corresponds with the infrared part of the electromagnetic spectrum. This means that a photon in the

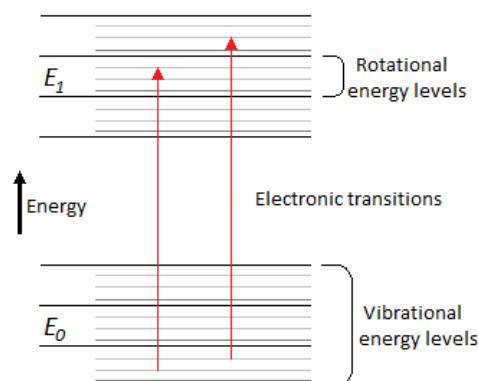
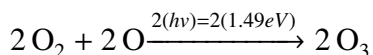
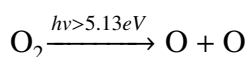


Figure 2.5: Schematic representation energy states of a molecule.

(near) infrared range can be a trigger for the molecule to vibrate. Molecules can also rotate, at all vibrational states there are different rotational states (J-states). Rotational motions are relatively easily excited and therefore are found in the far infrared and microwave range.

The molecules in the gas phase exhibit vibrations and rotation. But molecules in the solid state, like the molecules in ice, only show vibrations. These molecules do not have rotations because of the effect of the surrounding molecules. Therefore, to distinguish the different molecules in the ice infrared light is used. If a photon with the exact energy of the vibrational transition of the molecules in the ice interacts, the photon will be absorbed. But the photon will only get absorbed when the dipole moment of the molecule changes. Non-polar species, such as O<sub>2</sub> and N<sub>2</sub>, are infrared inactive and cannot be monitored using a pure vibrational mode.

To determine how many VUV photons per second arrive on the ice in an experiment O<sub>2</sub>-actinometry is used. An oxygen molecule consists of two oxygen atoms with each 8 electrons. When two oxygen atoms are bound one of the electrons in the outer shell get attracted to the nucleus of the other atom, the same applies for the electron of the other atom. It takes 5.13 eV to break the bond between these atoms, which is equal to a photon of 240 nm, this is called the binding energy. This bond can easily be broken by VUV light. When one free oxygen atom finds an oxygen molecule they can react and form ozone (O<sub>3</sub>) which has a dipole moment and therefore can be measured with FTIR. When the oxygen atom and molecule form ozone 1.49 eV (Karnarev and Normov) is released because the binding state has a lower energy.



A part of the energy of the first photon, to break the O<sub>2</sub> bond, is used for the bond of the third O atom in ozone  $(5.13 - (2 \cdot 1.49))/2 = 1.08$  eV. The bond energy (1.49 eV) of ozone is lower than the bond energy of an oxygen molecule, which means that an ozone molecule can be destroyed easier.

A thick ice (>500 ML) of oxygen molecules is formed on the substrate. All the photons must be absorbed to measure the absolute photon flux, that is why the ice has to be a thick layer. The ice will get irradiated by the ultraviolet light of the MDHL. An infrared spectrometer is used to record the O<sub>3</sub> absorption spectra (see chapter 3) at different intervals of irradiation. The oxygen ice is not visible in the absorption spectrum, but the increase of ozone over time can be measured. Ozone has a strong absorbance peak at 1040 cm<sup>-1</sup> that can be detected with the infrared spectrometer. To determine the absolute photon flux  $I_0$  (photon s<sup>-1</sup> cm<sup>-2</sup>) the next expression is used (Cottin et al., 2003):

$$I_0 = \frac{\Delta Area}{\Delta t \cdot QE \cdot A} \quad (2.2)$$

where  $\Delta Area$  is the increase of the area under the 1040 cm<sup>-1</sup> peak (cm<sup>-1</sup>),  $\Delta t$  the time since start of irradiation (s),  $QE$  the quantum efficiency of the formation of photoproducts in the ice (1.92 molecules photon<sup>-1</sup>) and  $A$  the band strength (1.4 x 10<sup>-17</sup> cm molecule<sup>-1</sup>) (Cottin et al. (2003) and references therein).



# Chapter 3

## Experimental

The experiments are conducted with different measuring techniques on the ‘CryoPAD 2’ (Cryogenic Photoproduct Analysis Device) setup. This setup exist of a main chamber, with a vacuum around  $10^{-11}$  mbar, in which interstellar ices are grown and photoprocessed. The ices are grown on a  $\text{MgF}_2$  transmission window that is attached on a “cold finger” cooled by a cryostat mounted on the top of the chamber. Also attached on the chamber is the microwave discharge hydrogen lamp that is the focus of the research in this thesis. The VUV light is directed towards the ice. Changes in the ice are studied by infrared light, with a Fourier Transform InfraRed (FTIR) spectrometer, and by a mass spectrometer. With the mass spectrometer the evaporated gas phase species of the ice after heating the sample can be detected. Recently also a VUV spectrometer is installed on the setup to study the ultraviolet light of the MDHL. Figure 3.1 shows a graphic design of the ‘CryoPAD 2’.

### 3.1 Detection techniques

With the Fourier Transform infrared spectrometer ( $500\text{-}4000\text{ cm}^{-1}$ ,  $0.5\text{ cm}^{-1}$  bandwidth) the absorption of ice in the infrared can be measured. The ice is deposited on a transmission window (section 3.4), that is cooled down to temperatures as low as 15 K, by a closed cycle He cryostat. The FTIR consists of an infrared light source that emits light through a Michelson interferometer with a moving mirror. The path of the beam outside the main chamber is completely covered and purged with water free dry air. This is to avoid all the absorption bands of water in the spectral range of the FTIR. After leaving the apparatus (figure 3.1[1]) the beam is focused by two gold mirrors in the purge box on to the ice sample (figure 3.1[7]). A part of the light gets absorbed by traveling through the ice, the remaining bundle is focused by one gold mirror on the MCT detector (figure 3.1[2]). The gold mirror and the MCT detector are both placed in a purge box. The detector is filled with liquid nitrogen to avoid thermal noise. An interferogram is made by measuring the signal at different positions of the mirror in the Michelson interferometer. The highest peak in the interferogram is when there is no path difference between the two beams. The intensity of the IR beam can be adjusted by an aperture at the exit when the light leaves the apparatus. The alignment of the mirrors is based on the maximum voltage of the interferogram. The computer program of the FTIR makes use of a Fourier Transform to get the spectrum. In the spectrum the absorption bands of the ice in this range can be seen.

The Quadrupole Mass Spectrometer is a Pfeiffer QMA200 and is connected to the main chamber (figure 3.1[3]) to measure the gas particles. The incoming gas particles get ionized and fragmented by a filament that emits electrons at 70 eV. The QMA consists of four rods that are placed parallel to each other. The opposing rods have the same voltage and the adjacent rods

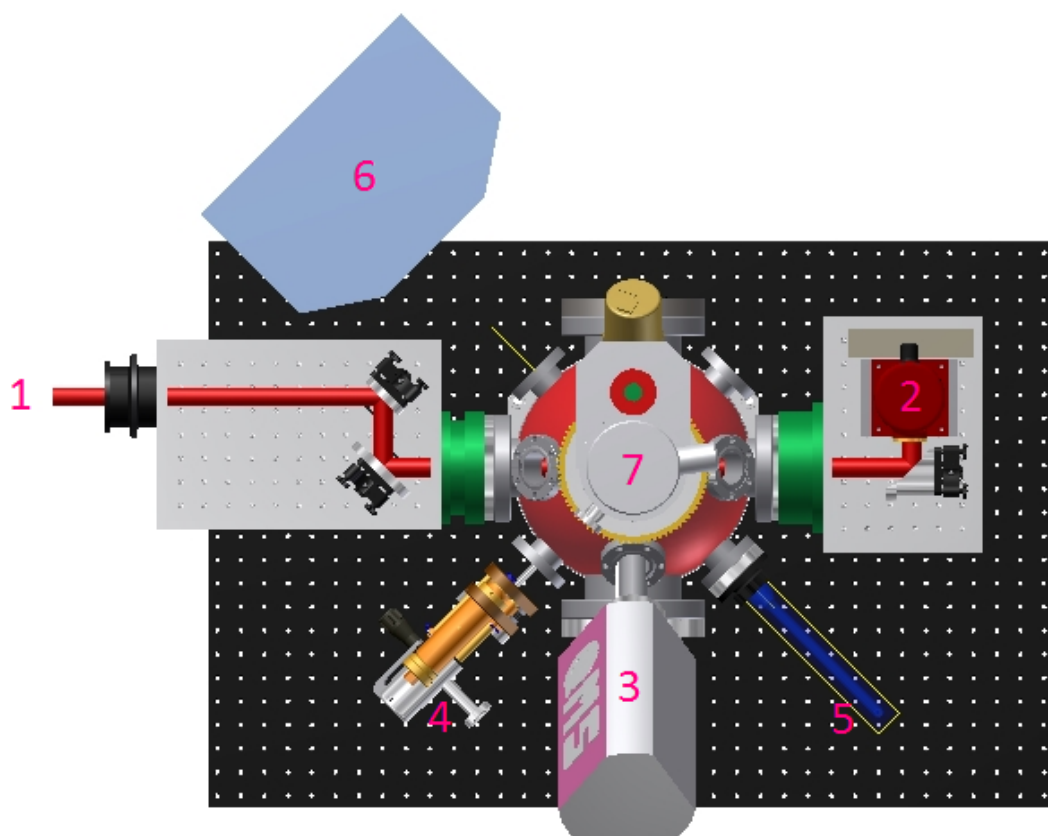


Figure 3.1: Top view of the main chamber with all the different equipment 1) exit of the FTIR where the bundle is coupled into the setup - 2) MCT detector of the FTIR - 3) QMS - 4) deposition line - 5) UV lamp - 6) VUV spectrometer and 7) place of the sample.

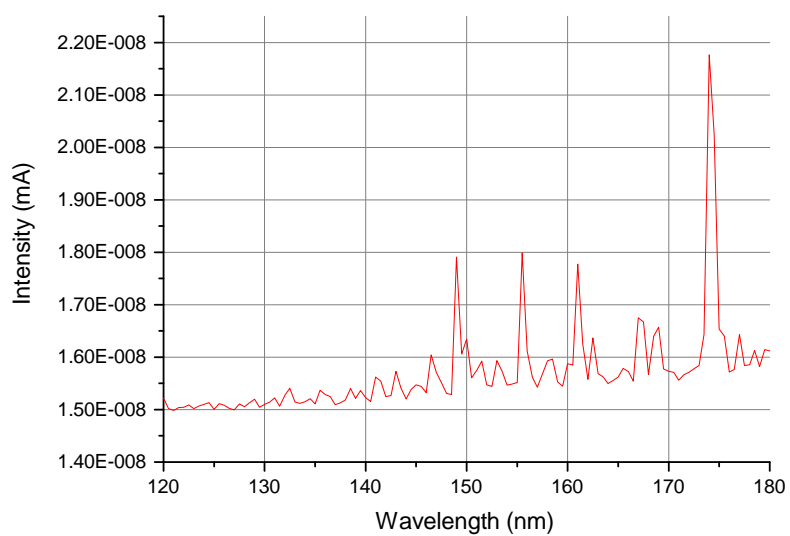


Figure 3.2: Spectrum of 0.5 mbar nitrogen, F-type lamp, HV of 300 V, slits 20 $\mu$ m-110 $\mu$ m.

are opposing in charge. The electric field generated by the rods guides charged particles to the detector. Depending on the mass and the charge ( $m/q$ ) of the particle it will reach the detector. By changing the voltage over the rods a specific  $m/q$  can be selected. The detector is a faraday cup. If the ion hits the cup, an avalanche of electrons gets produced and gives a current. It is not possible to measure all the masses in a short time with the Pfeiffer QMA200. To make the measurements faster only the masses that are interesting are selected.

## 3.2 VUV spectrometer

To measure the spectrum of the MDHL a vacuum ultraviolet spectrometer (figure 3.1[6]) is used. The spectrometer consists of a round chamber and two arms that form the connection to the main chamber and the Photo Multiplier Tube (PMT). A grating is located in the chamber and is attached to a rotation stage, which is controlled by the McPherson scan controller. The grating has 1200  $g/mm$  and stands 20 cm from the entrance and exit slit. An accuracy of 0.1 nm is possible over a range of 30 nm to 550 nm. With 10  $\mu m$  slits and 4 mm high the resolution amounts 0.1 nm with a spectral bandwidth of 0.8 nm. The dispersion of the beam is then 3.4 nm/mm. The PMT is attached at the exit of the VUV spectrometer. The high energy photons arrive at the scintillator. The scintillator transforms the high energy photons to lower energy photons by fluorescence. The produced photons loosen an electron in the photocathode, which is accelerated to a dynode with a higher potential and there releases more electrons. One photon is converted to more electrons after passing by all the dynodes and results in a current on the ammeter. This signal and the position of the grating gets saved by the program McPherson on the computer. With this program the data transform in to a spectrum. Because the grating has to move for measuring every wavelength, the measurement takes longer than a spectrometer that makes use of a CCD chip. The VUV spectrometer is used to detect the SED of the MDHL when running on CRYOPAD 2. However, here the system is used without connection to the main chamber, to study the MDHL directly.

## 3.3 UV lamp

To reproduce an UV field like in the interstellar medium use is made of a pyrex lamp (figure 3.1[5]). The lamp has three connections, see figure 3.3. Connection A is the connection to the main chamber, typically via a  $MgF_2$  window that serves as a vacuum seal. Connections B and C are used as gas in- and outlet, from a  $H_2$  gas bottle or mixing line and toward a vacuum pump. Connection B is connected to the gas bottle and connection C is connected to an oil pump which reaches a vacuum of  $10^{-2}$  mbar, measured nearby the gas bottle, when there is no gas in the lamp. A cavity which is connected to a microwave generator is attached to the lamp. The cavity is made of metal and conducts the microwaves through the lamp. Using a high voltage striker a plasma is initiated in the lamp. The free electrons and ions in the gas will accelerate

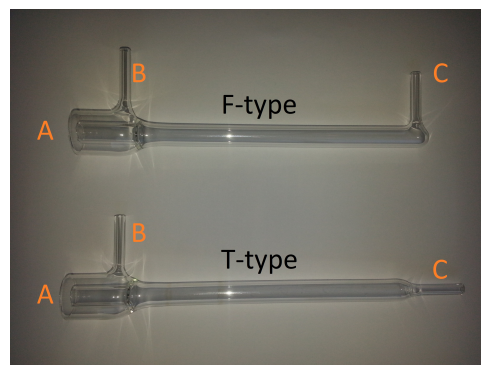


Figure 3.3: Microwave Discharge Hydrogen Lamp.

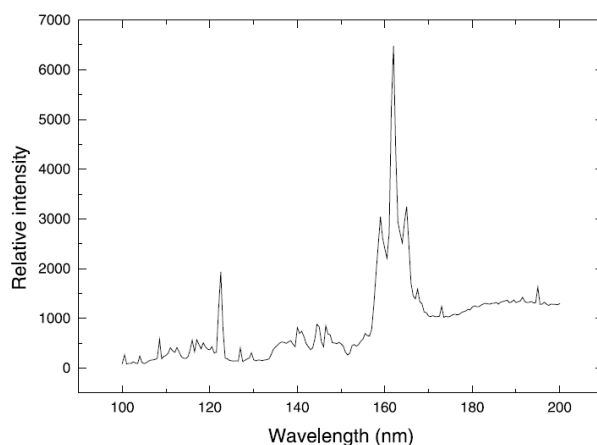


Figure 3.4: UV lamp spectrum at 1000 torr hydrogen with a lithium fluoride (LiF) window (Cottin et al. 2003).

and collide with other atoms. These atoms get excited to a higher energy level and decay by emitting a photon. Also the molecules get excited and emit photons. In order to prevent the lamp from melting it gets cooled by an airflow.

All experimental settings affect the spectrum of the lamp (Chen et al. (2014) and Ligterink et al. (2015 in prep.)). Different gases or gas mixtures have a different spectral response. Pure hydrogen gas has lines of the Lyman series and a molecular part in the ultraviolet range (figure 3.4).

But when hydrogen is mixed with helium, the molecular part of the hydrogen spectrum decreases and the Lyman- $\alpha$  peak increases because the helium separates the hydrogen atoms and counteracts the formation of hydrogen molecules. When nitrogen is used the spectral response is completely different, figure 3.2. The pressure of the gas in the lamp plays a role for the total flux and why some wavelengths are more intense than others. There are two types of the lamp: F-type and T-type. The shape could cause a difference in the spectrum because the gas flow in the lamp is different. The position of the cavity has a small effect on the spectrum. The plasma is produced on the place of the cavity, but the lamp can be seen as a point source at connection A. Also the voltage of the microwave and the pumping efficiency can affect the total flux.

## 3.4 Samples

The deposition line (figure 3.1[4]) is connected to a gas mixing line. This deposition line can be moved in and out of the main chamber. Gas will enter the main chamber through the deposition line. A micro capillary plate at the end of the line limits the gas beams divergence. The sample is a  $\text{MgF}_2$  window that is connected to the cold finger. The beam of the FTIR travels through the  $\text{MgF}_2$  window and the ice. The cold finger gets cooled by the cryostat, that works with the expansion of helium. The cryostat can be cooled to  $\sim 10$  K. To regulate the temperature of the substrate a heater is also connected to the cold finger.

### 3.4.1 Background deposition

One of the methods to make an ice layer on the substrate is by background deposition. The deposition line is not aligned toward the center of the main chamber, which is the case for direct deposition, but is placed at the wall. The sample is rotated perpendicular with the deposition

line. The gas spreads throughout the main chamber and will stick on all the cold surfaces. The growth of the ice layer is determined by the Langmuir equation. One Langmuir ( $L$ ) is equal to the coverage of one monolayer on all the cold surfaces:

$$L = 10^6 \cdot P_m \cdot t \quad (3.1)$$

where  $P_m$  is the pressure in the main chamber and  $t$  the time of deposition. During the deposition it should be taken into account that a pressure higher than  $10^{-5}$  mbar can be harmful for the QMS and the turbo pump.

### 3.4.2 Direct deposition

Normally the deposition takes place when the deposition line is aligned to the center of the main chamber, right in front of the substrate. When the gas flows in the main chamber, most of the gas will stick on the transmission window, because this is near by the outflow. The thickness of the ice depends of the local pressure at the window and the time of the deposition. Most ices for photodesorption, photodestruction and photochemistry experiments have a dipole moment and therefore can be seen in the infrared absorbance spectrum. The thickness of the ice can be calculated as follows (Muñoz Caro et al., 2010):

$$N = \frac{2.3 \cdot Area}{A} \quad (3.2)$$

where  $N$  is the column density of the measured surface (molecules  $\text{cm}^{-2}$ ),  $Area$  is the area under the infrared peak of the ice ( $\text{cm}^{-1}$ ) and  $A$  is the band strength of the specific peak ( $\text{cm molecules}^{-1}$ ). With the column density the number of monolayers can be determined.

When the ice has no dipole moment, the equation above cannot be used. But when it is a really thick ice ( $>500$  ML) an interference pattern can be detected in the absorbance spectrum. Thick ice will work like a Fabry Perot interferometer, what means that the light will reflect on the inside edges of the ice and will interfere with itself. To calculate the thickness of the ice the next equation is used (Dartois et al., 2004):

$$d_{ice} = \frac{1}{2\Delta\nu n_{ice}} \quad (3.3)$$

where  $d_{ice}$  is the thickness of the ice (cm),  $\Delta\nu$  is the wavenumber difference between the minima or maxima ( $\text{cm}^{-1}$ ) and  $n_{ice}$  is the refractive index of the ice. With the thickness, the number of monolayer can be calculated:

$$N_{mono} = \frac{N_A d_{ice} \rho_{ice}}{m_{ice}} \quad (3.4)$$

where  $N_{mono}$  is the number of monolayers,  $N_A$  Avogadro's number ( $6.022 \times 10^{23} \text{ mol}^{-1}$ ),  $\rho_{ice}$  the density of the ice ( $\text{g cm}^{-3}$ ) and  $m_{ice}$  the molar mass ( $\text{g mol}^{-1}$ ).



# Chapter 4

## Results

In this chapter the results of the measurements on the MDHL are discussed. Three different measurements were performed that provide information about the spectrum and the photon flux of the MDHL.

### 4.1 Measured VUV spectra

Ligterink et al. (2015 in prep.) show the spectrum of a MDHL with 0.5 mbar hydrogen, figure 4.1. This spectrum is measured on a calibrated VUV monochromator with a bandwidth of 1.6 nm and a step size of 0.5 nm. In this spectrum the Lyman- $\alpha$  peak is three times higher than the molecular part of the spectrum. In the laboratory the spectrum of the MDHL is measured with the uncalibrated VUV spectrometer. The lamp is directly attached to the spectrometer with an MgF<sub>2</sub> window in between. The pressure gauge for the spectrometer is placed before the entrance slit, because that is the place of the highest pressure. First the spectrometer was pumped by an oil pump, reaching a pressure of  $\sim 10^{-3}$  mbar. In the measured spectra it was found that the Lyman- $\alpha$  peak was much less intense than the molecular part of the spectrum (figure 4.2) and moreover decreases over time. However, this does not correspond with the data of Ligterink et al. (2015 in prep.). A logical explanation is that the pressure in our spectrometer is higher, so a part of the Lyman- $\alpha$  gets absorbed by gas phase or deposited material. This will be discussed later in this section. Replacing the oil pump with a turbo resulted in a lower vacuum of  $10^{-4}$  mbar (limited by the fact that the VUV spectrometer was pumped through a 1 m long and narrow tube). While the pump was replaced, the MgF<sub>2</sub> window was also removed for cleaning. It appeared that there was dirt on the window on both sides. This could also be a reason why the Lyman- $\alpha$  peak was lower than expected. The origin of this dirt was not a priori clear and may be linked to oil pollution as well as photochemical surface reactions due to background gas. It should be noted that this problem did not appear when the system was mounted onto the UHV setup (Ligterink et al., 2015 in prep.).

After the pump was replaced, new spectra were taken over time. It turned out that the Lyman- $\alpha$  indeed increased to three times higher than the molecular part because of the lower pressure in the spectrometer. But it still decreases over the time of irradiation, see figure 4.3.

Decreases in both the Lyman- $\alpha$  peak (121.2-121.7 nm) and the molecular part (135.0-170.0 nm) are visualized by dividing their integral values by the first value in the data series. This means that the first value is one, since it is divided by itself and other data points show a percentage wise deviation with respect to the first data point. This enables us to visualize trends in and between both spectral parts. In figure 4.4 it is shown that the Lyman- $\alpha$  peak decreases with 27% over a time span of 90 minutes, while the molecular part seems to be relatively stable.

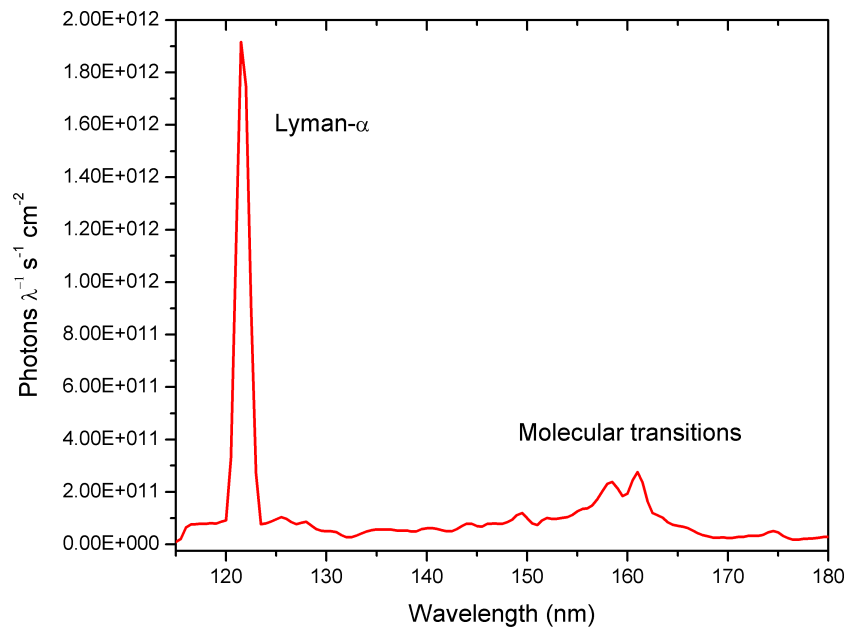


Figure 4.1: Flux calibrated spectrum of 0.5 mbar hydrogen, bandwidth of 1.6 nm and a step size of 0.5 nm (Ligterink et al., 2015 in prep.).

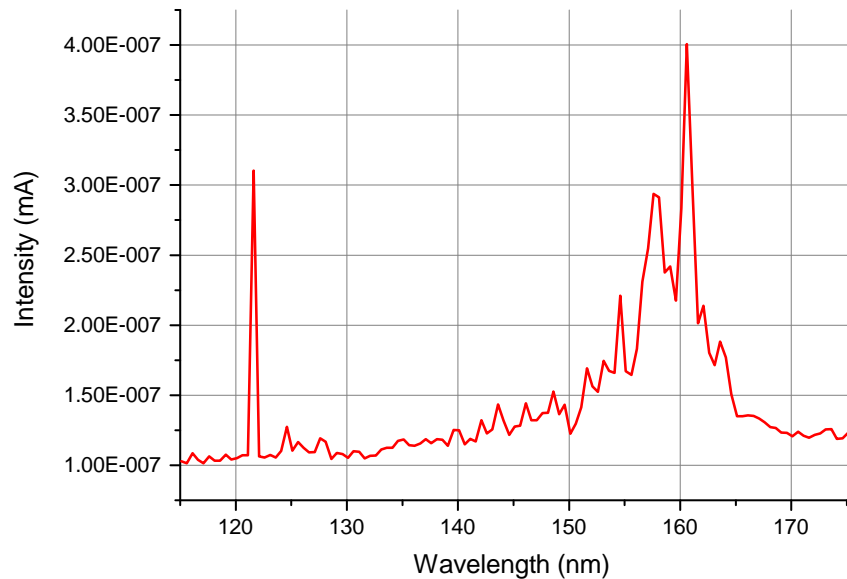


Figure 4.2: Spectra measured with the VUV spectrometer of 0.5 mbar hydrogen, a step size of 0.5 nm and a pressure of  $10^{-3}$  mbar in the spectrometer. Here is seen that the Lyman- $\alpha$  peak is much less intense than the molecular part.

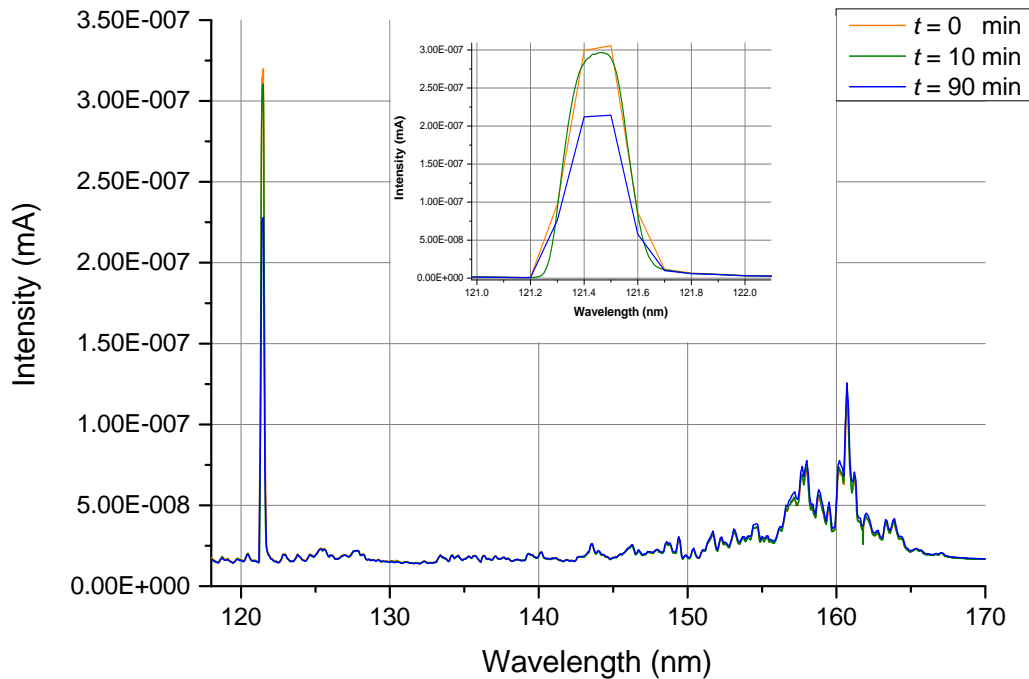


Figure 4.3: Spectra of the UV-lamp at 0.5 mbar hydrogen, F-type lamp,  $10^{-4}$  mbar spectrometer, HV of 300V, slits  $20\mu\text{m}$ - $80\mu\text{m}$ .

Ligterink et al. (2015 in prep.) find that the Lyman- $\alpha$  increases 3% in the first 5 minutes and the molecular part decreases 1% in the first 5 minutes, an effect ascribed to thermal settling. However, after the first 5 minutes both spectral contributions are stable over a long time. This means something else affects the spectrum over the time in these measurements.

It seems that the layer of dirt forms during the irradiation. Another experiment is done to test if this is true and what kind of impact it has on the spectrum. The experiment starts with a clean window on both sides. When the MDHL is turned on, five spectra are taken for different irradiation times. After these measurements the MDHL is turned off and the outside (the side of the MDHL) is cleaned. Next, the MDHL was turned on and again five spectra were taken. This is repeated three times. The pressure in the lamp is 0.5 mbar, the high voltage is 300 V and the pressure in the spectrometer is  $9.0 \cdot 10^{-5}$  mbar.

In figure 4.5a the integrated area under the Lyman- $\alpha$  peak is plotted against the time of irradiation. Three lines are plotted. At the first measurement the window is cleaned on the inside and outside and after the cleaning the spectrometer and lamp are pumped over the weekend. The second and third line are the measurements after cleaning only the outside of the window and before the measurement the lamp is only pumped for a few minutes. In all three measurements the Lyman- $\alpha$  peak decreases over the time of irradiation, but after cleaning the outside of the window the Lyman- $\alpha$  peak increases a bit. The increase of the peak after cleaning is an evidence that the layer of dirt affects the spectrum. The peak does not increase to the point where it started, which means that there is also a layer of dirt formed on the other side of the window.

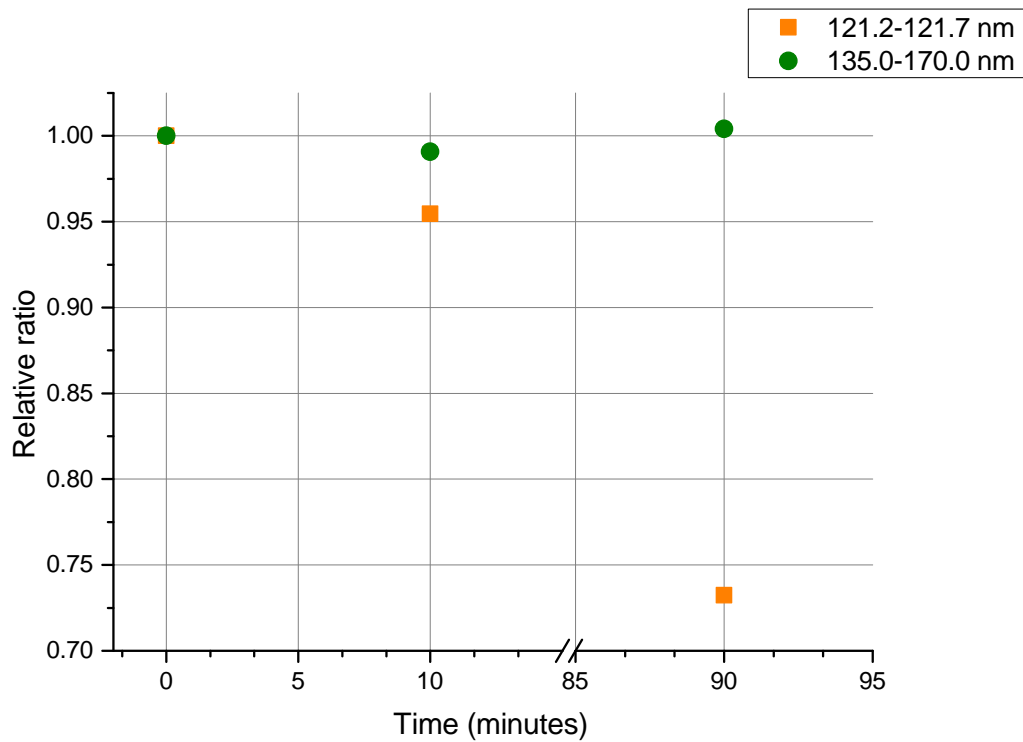


Figure 4.4: Relative ratio over the time of Lyman- $\alpha$  and molecular at 0.5 mbar hydrogen, F-type lamp,  $10^{-4}$  mbar spectrometer, HV of 300 V, slits  $20\mu\text{m}$ - $80\mu\text{m}$ .

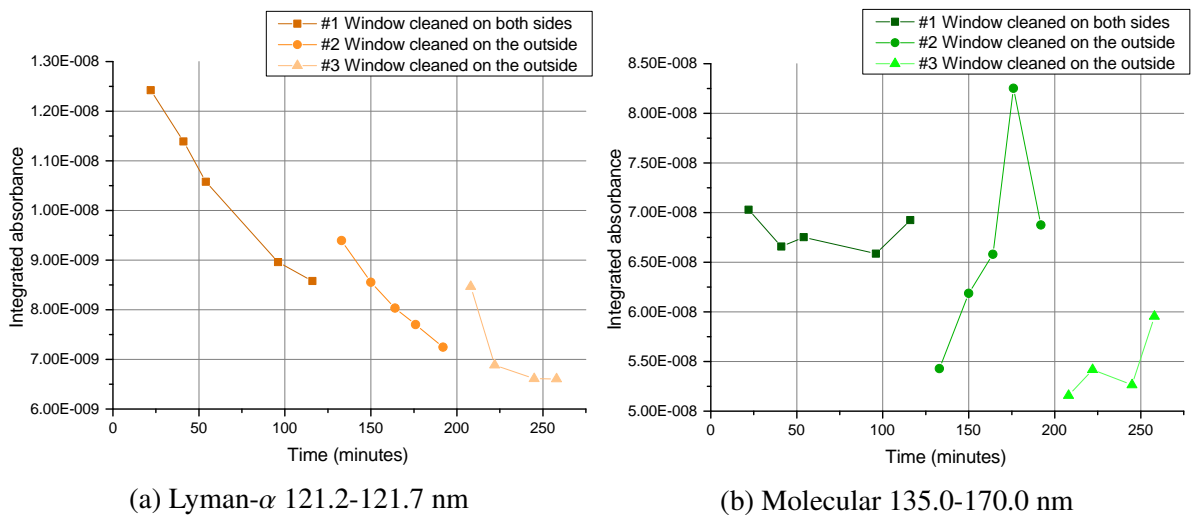


Figure 4.5: Intensity at 0.5 mbar hydrogen, F-type lamp,  $9 \cdot 10^{-5}$  mbar spectrometer, HV of 300 V, slits  $20\mu\text{m}$ - $80\mu\text{m}$ .

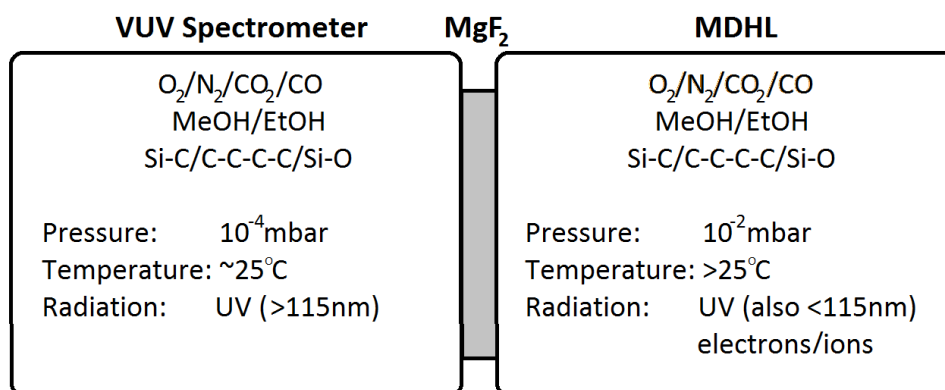


Figure 4.6: Gas phase conditions in the spectrometer and in the MDHL.

The molecular part of the spectrum shows a different pattern. Instead of decreasing over time of irradiation, the molecular part seems to increase, see figure 4.5b. It seems that the first measurement is fluctuating around a horizontal line, this is the measurement where the spectrometer and lamp are pumped over the weekend. After cleaning the window the molecular part decreases and during the irradiation it seems that it increases to the horizontal line of the first measurement. The same applies for the third measurement. It seems that because of the cleaning something deposits on the window that absorbs the molecular part. This effect is not seen at the Lyman- $\alpha$  peak, so it is something that only absorbs the molecular part and not the Lyman- $\alpha$ . The bonding between the product that blocks the molecular part and the window should not be strong, because it can be pumped away at a pressure of 10<sup>-2</sup> mbar. It can also be removed by the heat of the plasma in combination with the intense ultraviolet radiation. The window is cleaned with methanol and ethanol, these substances are not completely pure, what means that they are contaminated with water. It could be that the water bonds with the MgF<sub>2</sub> and absorbs the molecular part.

The layer of dirt that has been formed on the window exists of particles present in the vacuum. For both the spectrometer as the MDHL there are still air molecules in the vacuum. The window is cleaned with methanol and ethanol, so remnants of these substances could be in the spectrometer and the MDHL. The MDHL is pumped by an oil pump, what means that there could be oil in the vacuum. Before the turbo pump was used for the spectrometer it was pumped by an oil pump, what could cause that there are still remnants of oil in the spectrometer. In figure 4.6 the conditions of the spectrometer and the MDHL are visualized. These conditions, could influence the kind of dirt that is produced on both sides and result in different effects on the VUV transmission and explain the different behavior seen in the spectrum. More measurements need to be done to clarify how it is influenced.

So in summary, for the specific settings used here, it is important to note that pollutions can influence the emission pattern of the lamp. As obvious this may sound, this has not been systematically investigated over the years (with exception of Chen et al. (2014) and Ligterink et al. (2015 in prep.)). It has been generally known that with time fluxes decrease, but it has not been taken into account that the actual wavelength pattern also varies. This is an important finding, as in recent years (see e.g. Fayolle et al. (2011)) it has become clear that solid state photoprocessing can be highly wavelength dependent.

Table 4.1: Settings of the three  $^{18}\text{O}_2$ -actinometry measurements with a T-type lamp and using a collimating tube in the main chamber.

Measurement	$P_{cham}$	$P_{lamp}$	Gas	$\angle$ IR	$\angle$ UV
1	$10^{-11}$ mbar	0.5 mbar	$\text{H}_2$	$270^\circ$	$225^\circ$
2	$10^{-11}$ mbar	4.0 mbar	$\text{H}_2$	$270^\circ$	$225^\circ$
3	$10^{-9}$ mbar	1.43 mbar	$\text{H}_2/\text{He}$ (1:4)	$270^\circ$	$225^\circ$

## 4.2 $\text{O}_2$ -actinometry measurements

The absolute flux of the MDHL with different settings is measured using  $\text{O}_2$ -actinometry on the CryoPAD 2 setup. In this section three measurements will be discussed. The results of other measurements are shown in Appendix A, but these are not relevant to the comparison made in this section. The three measurement are performed for the same conditions except that in between the second and last measurement the turbo pump of the main chamber broke down and had to be replaced with a lower capacity pump (1000 l/s vs 250 l/s). The pressure in the main chamber with the old pump was  $\sim 10^{-11}$  mbar and with the replacement pump it was  $\sim 10^{-9}$  mbar. This should not affect the results, because thick ices are used.  $^{18}\text{O}_2$  is used for the experiments. This assures that eventual background gas pollution by regular  $\text{O}_2$  can be excluded. The absorption peak in the infrared of  $^{18}\text{O}_3$  is a bit shifted with respect to the absorption peak of  $\text{O}_3$ . Because it is a small shift the quantum efficiency and band strength of the  $1040\text{ cm}^{-1}$  absorption peak can be used. The settings of the three measurements can be found in table 4.1.

The recording of an infrared spectrum and the irradiation of the ice cannot take place at the same time. When the sample stands perpendicular on the UV radiation the sample holder blocks the path of the infrared beam. And when the sample stands perpendicular on the path of the infrared beam, the ice is not completely irradiated. That is why the lamp is turned on and off during the experiment while the sample gets rotated, see Appendix B. The lamp is warmed up for 15 minutes, so the flux is stable during the measurement. For the deposition the deposition line is placed close to the sample and it is assumed that with a pressure of  $1 \times 10^{-9}$  mbar in the main chamber the ice will grow with one monolayer per minute. This is based on isothermal CO desorption experiments and is not very accurate, but a good assumption for thick ices. For the first two measurements an ice of around 500 ML is deposited and for the last measurement an ice of around 2500 ML is deposited, because here the pressure in the main chamber is higher. During the experiments the temperature of the cold finger was 17 K. The ice gets irradiated for 20 minutes in total. At the beginning every minute a spectrum with the FTIR is taken and after 10 minutes the spectra were taken every 5 minutes.

In figure 4.7 the absorption peak of the ozone is plotted, for experiment 2. The absorption peak increases over the time of irradiation, meaning that ozone gets formed. The bands are integrated between  $968.7\text{ cm}^{-1}$  and  $994.1\text{ cm}^{-1}$  so that the growth of ozone can be plotted against time (figure 4.8). The formation of ozone starts linearly, but after the first minutes the oxygen gets depleted and less ozone will be formed. To calculate the total flux, the linear part of the ozone formation must be determined. To do this an exponential fitted curve is used, that derives the slope of the linear curve at the beginning. The coefficient of determination for the exponential fit amounts 99%. With one measurement the standard deviation can not be determined. Here fore, the measurements have to be repeated. The main uncertainties here are caused by the accuracy with which the irradiation time is determined as well as variations in the gas pressure

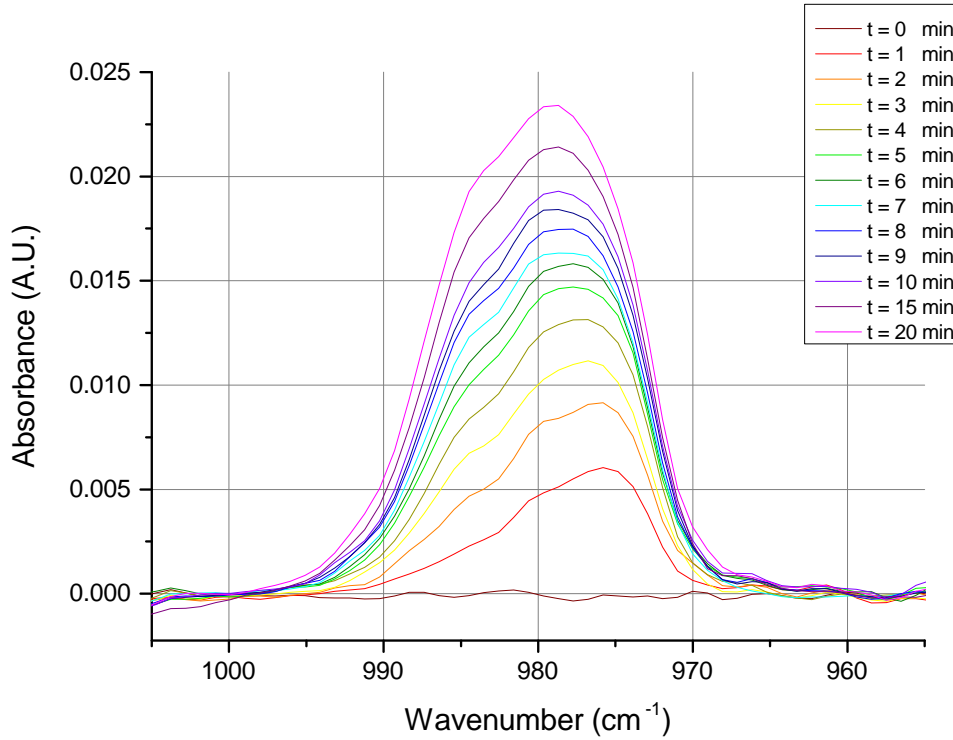


Figure 4.7: The absorption peak of ozone (measurement 2) over time of irradiation in minutes.

Table 4.2: Determined fluxes with actinometry ( $\phi_a$ ) and fluxes of Ligterink et al. (2015 in prep.) ( $\phi_L$ ).

Measurement	$\phi_a$ (photons $s^{-1} cm^{-2}$ )	$\phi_L$ (photons $s^{-1} cm^{-2}$ )
1	$3.59 \cdot 10^{13}$	$9.0 \cdot 10^{12}$
2	$3.39 \cdot 10^{13}$	$6.1 \cdot 10^{12}$
3	$1.23 \cdot 10^{13}$	$8.6 \cdot 10^{12}$

can be controlled. The standard deviation can also be caused by the inaccuracy of the thickness of the ice, fluctuations of the temperature of the sample and fluctuations of the pressure in the main chamber. As seen in figure 4.8 the two measurements with hydrogen are close to each other while the measurement with the hydrogen helium mixture has a much lower absorbance. With the aid of equation 2.2 and the determined slope the fluxes can be calculated and are shown in table 4.2. Ligterink et al. (2015 in prep.) discuss the spectra for the same settings as used by the actinometry measurements, see figure 4.9. The only difference is that for the 4.0 mbar hydrogen measurement there is made use of a F-type lamp instead of a T-type lamp that has been used for all the actinometry measurements. For the actinometry experiments also use is made of a collimating tube located in the main chamber. The absolute fluxes of the measurements in Ligterink et al. (2015 in prep.) are determined with a NIST calibrated photodiode at a distance of 38 cm and are shown in table 4.2.

The fluxes recorded here and by Ligterink et al. (2015 in prep.) are normalized to their highest flux for a comparison. In figure 4.10 the normalized fluxes are plotted against the normalized molecular part of the spectrum from Ligterink et al. (2015 in prep.). As seen in this figure the values are not close to each other. When the molecular part decreases about 60 % relative to the highest molecular part, the total flux of the actinometry differs about 60% of Ligterink et al. (2015 in prep.). And when the molecular part is the highest, the flux of the actinometry lies

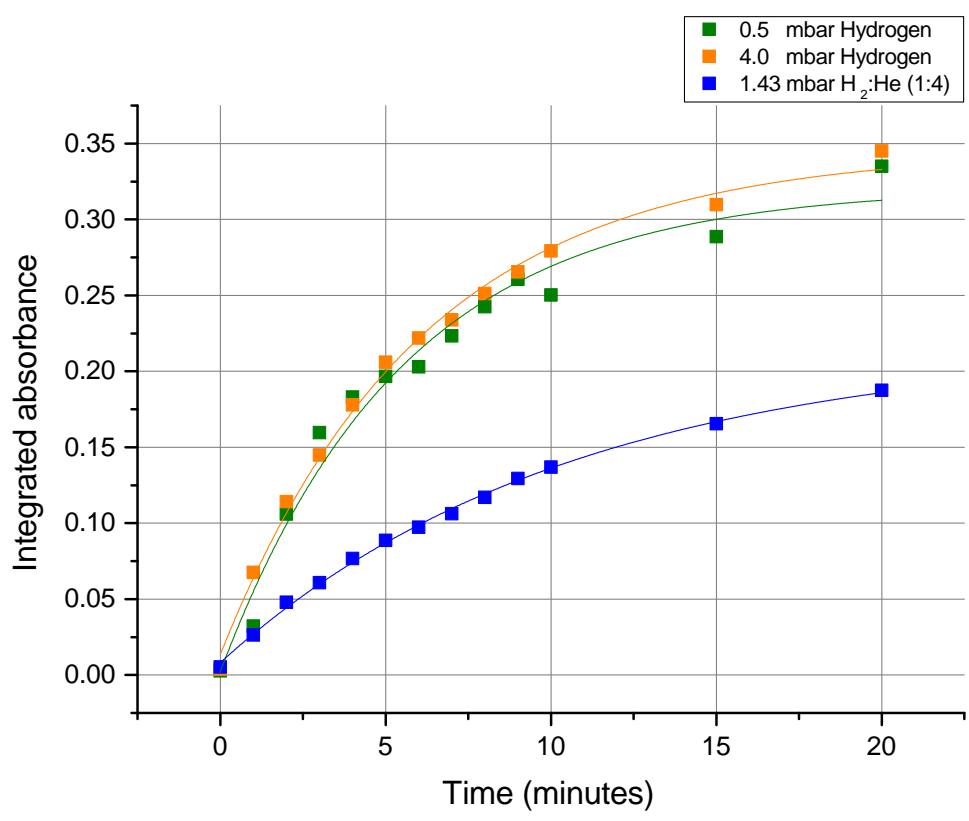


Figure 4.8: The increase of ozone over the time of irradiation, for measurement 1, 2 and 3.

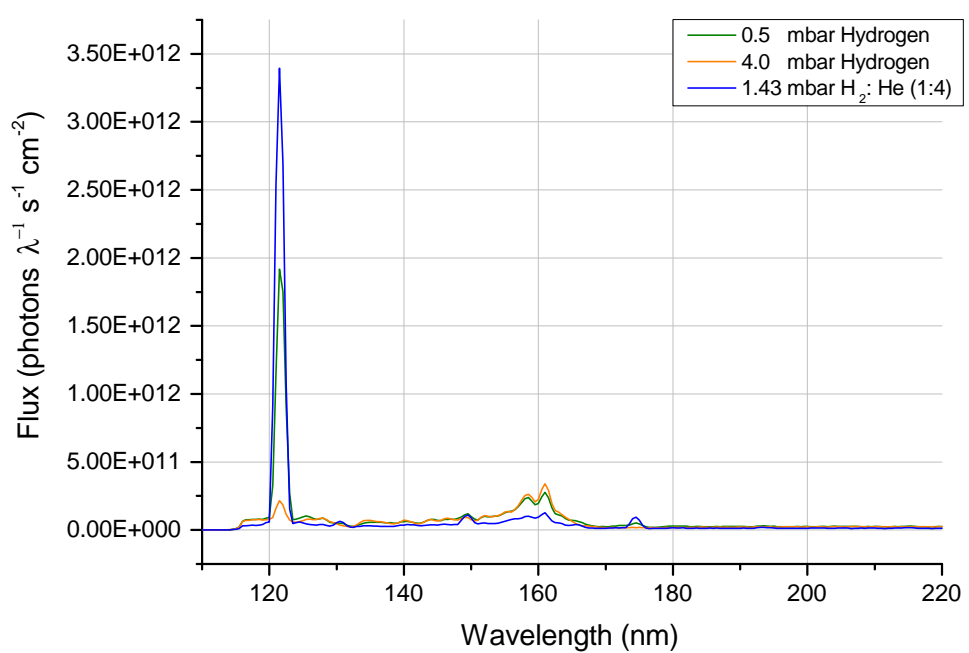


Figure 4.9: Spectra recorded with a calibrated spectrometer (Ligterink et al., 2015 in prep.).

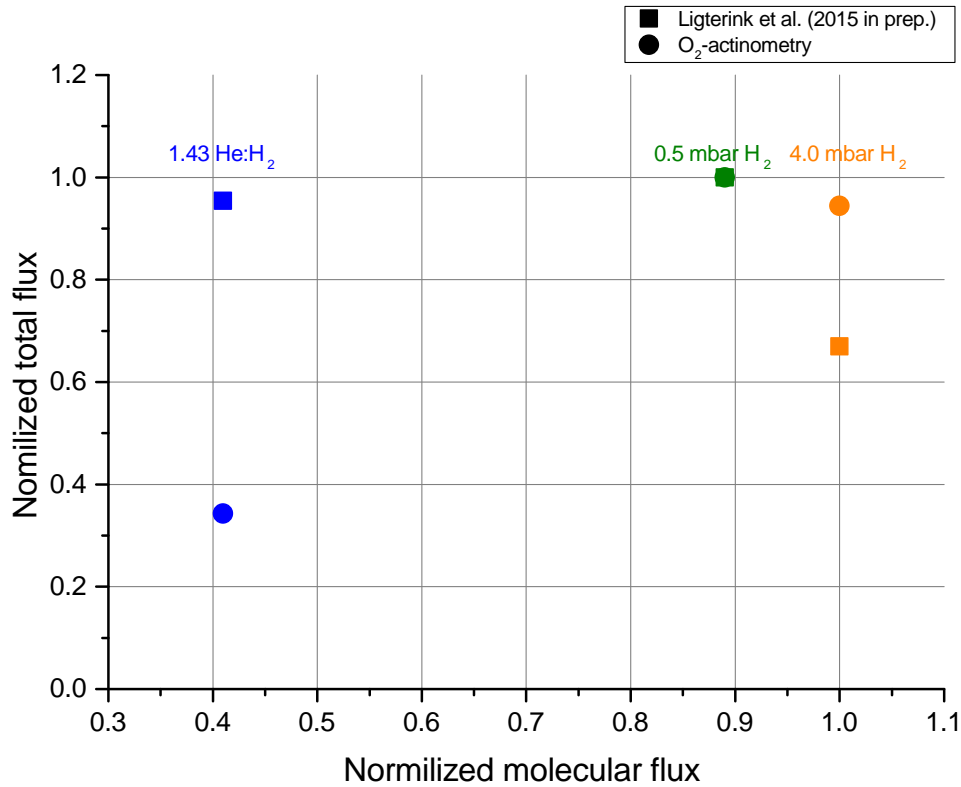


Figure 4.10: Normalized flux of the O<sub>2</sub>-actinometry experiments and the fluxes of Ligterink et al. (2015 in prep.) relative to the normalized molecular part of the spectrum (155-165 nm).

around 30% higher than Ligterink et al. (2015 in prep.). The measured fluxes of Ligterink et al. (2015 in prep.), however, are not wavelength dependent and consequently, what means that the fluxes of the O<sub>2</sub>-actinometry experiments are more sensitive for the molecular part as for Lyman- $\alpha$ . Cruz-Diaz et al. (2014) already showed that the absorption cross section for O<sub>2</sub> ice is higher for 160 nm than around 121 nm. The wavelength dependence of O<sub>2</sub>-actinometry has a big effect of the flux that is measured and is therefore not a good way to measure the absolute photon flux. However this is a good method to get an idea of the order of magnitude of the flux during the photodesorption, photodestruction and photochemistry experiments.

### 4.3 UV/VIS spectrometer

The intensity of the Lyman lines, and thus also Lyman- $\alpha$ , is related to the intensity of the Balmer lines (figure 2.4). To investigate the relation between Lyman and Balmer lines another setup is used. The MDHL is placed one meter in front of the entrance slit of an UV/VIS spectrometer. In this spectrometer the light falls on a grating that disperses the light in the different wavelengths. The dispersed light comes parallel on a CCD sensor with the aid of two mirrors. The specifications of this sensor tell that every photon creates 14 counts in the spectrum. The lamp is separated from the air with an MgF<sub>2</sub> window. After the light leaves the lamp it travels through the air, but the visible part of the spectrum will not be absorbed significantly, but VUV (Vacuum UltraViolet) photons will be completely absorbed. In figure 4.11 the detected spectrum of the MDHL with 0.4 mbar hydrogen is visualized. In this spectrum the Balmer lines are visible.

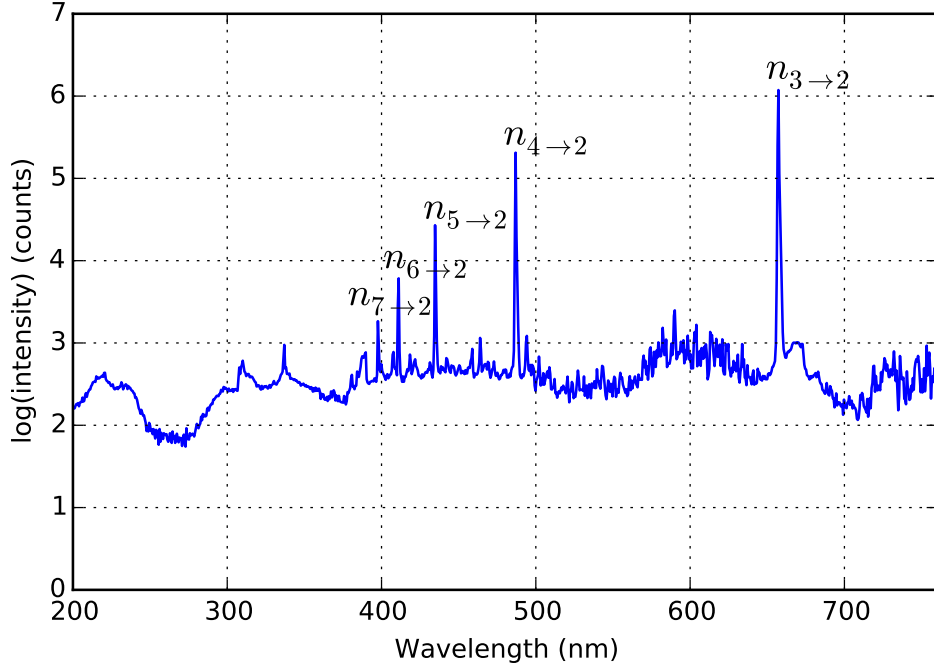


Figure 4.11: Spectrum of the MDHL at 0.4 mbar Hydrogen. The different Balmer lines are indicated.

Table 4.3: Einsteins efficiency coefficients for several transitions per second (Berestetzki et al.).

level	2 ( $\cdot 10^8 \text{ s}^{-1}$ )	3 ( $\cdot 10^8 \text{ s}^{-1}$ )	4 ( $\cdot 10^8 \text{ s}^{-1}$ )	5 ( $\cdot 10^8 \text{ s}^{-1}$ )	6 ( $\cdot 10^8 \text{ s}^{-1}$ )
1	4.6966948	0.55727384	0.12779603	0.041232986	0.01643335
2		0.4408291	0.084157168	0.025293477	0.0097278027
3			0.089822794	0.021998225	0.0077795773
4				0.026981317	0.0077077669
5					0.010249685

Table 4.4: Temperature calculation with the intensity of the Balmer lines.

(a) 0.4 mbar hydrogen

States	$I_c$ (counts)	$\phi$ (photons $s^{-1}$ )	$N_{n_x}$	$T$ (K)
$n_3 \rightarrow n_2$	$1.18 \cdot 10^6$	$6.49 \cdot 10^8$	14.7	
$n_4 \rightarrow n_2$	$2.04 \cdot 10^5$	$6.10 \cdot 10^7$	7.25	$5.98 \cdot 10^3$
$n_5 \rightarrow n_2$	$2.69 \cdot 10^4$	$6.85 \cdot 10^6$	2.71	$2.48 \cdot 10^3$
$n_6 \rightarrow n_2$	$6.11 \cdot 10^3$	$1.47 \cdot 10^6$	1.51	$2.04 \cdot 10^3$

(b) 0.8 mbar hydrogen

States	$I_c$ (counts)	$\phi$ (photons $s^{-1}$ )	$N_{n_x}$	$T$ (K)
$n_3 \rightarrow n_2$	$1.42 \cdot 10^6$	$7.82 \cdot 10^8$	17.7	
$n_4 \rightarrow n_2$	$3.09 \cdot 10^5$	$9.24 \cdot 10^7$	11.0	$7.27 \cdot 10^3$
$n_5 \rightarrow n_2$	$4.24 \cdot 10^4$	$1.08 \cdot 10^7$	4.26	$2.55 \cdot 10^3$
$n_6 \rightarrow n_2$	$9.45 \cdot 10^3$	$2.28 \cdot 10^6$	2.34	$2.01 \cdot 10^3$

(c) 1.2 mbar hydrogen

States	$I_c$ (counts)	$\phi$ (photons $s^{-1}$ )	$N_{n_x}$	$T$ (K)
$n_3 \rightarrow n_2$	$1.52 \cdot 10^6$	$8.34 \cdot 10^8$	18.9	
$n_4 \rightarrow n_2$	$3.47 \cdot 10^5$	$1.04 \cdot 10^8$	12.3	$7.64 \cdot 10^3$
$n_5 \rightarrow n_2$	$4.85 \cdot 10^4$	$1.23 \cdot 10^7$	4.88	$2.59 \cdot 10^3$
$n_6 \rightarrow n_2$	$1.08 \cdot 10^4$	$2.61 \cdot 10^6$	2.68	$2.00 \cdot 10^3$

During the experiments use is made of hydrogen gas in a F-type lamp. There are three measurements done with different pressures at 0.4 mbar, 0.8 mbar and 1.2 mbar. The flux of the different peaks over the time is calculated in photons per second ( $\phi$ ) using:

$$\phi = \frac{I_c}{14 \cdot t_s \cdot g} \quad (4.1)$$

where  $I_c$  is the intensity in counts and  $t_s$  is the shutter time of the CCD sensor. The absorption of the coating on the grating is wavelength dependent and included in the calculation, by variable  $g$ . The convert counts into photons the factor 14 is used. The measured intensity in counts and the calculated fluxes are shown in table 4.4. The chance that the electrons in the  $n_x$ -state ( $x=2,3,4,\dots$ ) decay to a lower state is known for several transitions, table 4.3. The population  $N_{n_x}$  in the  $n_x$ -state can be calculated, with the flux of the lines from table 4.4, with the following equation:

$$N_{n_x} = \frac{\phi(x)}{a(x)} \quad (4.2)$$

where  $\phi$  is the flux (photons  $s^{-1}$ ) of one of the Balmer lines and  $a(x)$  the chance of decay at that specific line (photons  $s^{-1}$ ). The distribution of the electrons in the energy levels follows a Boltzmann distribution. With the population in the different energy states the temperature of the plasma can be calculated with the equation of the Boltzmann distribution.

$$\frac{N_{n_2}}{N_{n_1}} = \frac{g_2}{g_1} \exp\left(-\frac{E_2 - E_1}{kT}\right) \quad (4.3)$$

where  $g$  is the degeneracy of the different energy levels  $n_2$  and  $n_1$ ,  $E$  the energy of the different levels in (J),  $k$  the Boltzmann constant ( $1.38 \times 10^{-23}$  J/K) and  $T$  is the kinetic temperature (K).

Table 4.5: Calculated Lyman- $\alpha$  flux with the average temperature.

$P_{MDHL}$ (mbar)	$T_{gem}$ (K)	$N_{n_2}$	$\phi$ (photons s <sup>-1</sup> )
0.4	$3.50 \cdot 10^3$	$3.44 \cdot 10^3$	$1.62 \cdot 10^{12}$
0.8	$3.94 \cdot 10^3$	$2.05 \cdot 10^3$	$9.65 \cdot 10^{11}$
1.2	$4.08 \cdot 10^3$	$1.82 \cdot 10^3$	$8.57 \cdot 10^{11}$

The temperature is calculated for several populations, table 4.4. The values of the temperature between the different states have large differences. The quantum efficiency of the CCD of the spectrometer is not taken into account and differs for the several Balmer lines. This could be an effect why the calculated temperatures differs. The temperatures can also differ if the gas is not in a thermal equilibrium. In order to take all the values in the calculation, the average of the different temperatures is used, table 4.5. Now that the average temperature of the plasma is known, the population in the  $n=2$  state can be calculated with equation 4.3. And with this population the flux of the Lyman alpha line can be calculated with equation 4.2. The results of these calculations are found in table 4.5.

The measured spectra in Ligterink et al. (2015 in prep.) showed that the Lyman- $\alpha$  peak decreases when the pressure in the MDHL increases. As seen in table 4.5 the flux of the Lyman- $\alpha$  peak also decreases at higher pressures. Because only three measurements are done, the reliability of the Lyman- $\alpha$  fluxes is not high. To make a better judgment about the Lyman- $\alpha$  fluxes, more measurements are needed.

The calculated fluxes of the Lyman- $\alpha$  peak are not fully identical to the flux that is experienced by the sample during the photodesorption, photodestruction and photochemistry experiments. A part of the intensity of the Balmer lines is absorbed by the MgF<sub>2</sub> window. The amount of absorbance is wavelength dependent and also depends on the thickness of the window. The intensity of the Lyman- $\alpha$  line is calculated for the same absorption as the Balmer lines. However, the absorption of the window for Lyman- $\alpha$  is much bigger. This means that the flux is lower than calculated. Another difference is that the distance between the lamp and the spectrometer is larger than the distance between the lamp and the sample. Because the distance to the spectrometer is bigger, the measured flux should be lower at the sample.

### 4.3.1 Color fluctuations

Normally the flux and color of the MDHL lamp is stable over time. It is known that when the lamp is switched on, the flux starts high and stabilizes after 5 minutes. But sometimes during the experiment the lamp changes color. Normally it is pink for the human eye (figure 4.14) and then it turns white. This did also happen during the measurements of the Balmer lines. Figure 4.12 is a 3D graphic of the spectra over the time. In this figure the point where the color of the lamp changes is indicated with a vertical line. At that point the intensity of the Balmer lines decreases and three new peaks are formed. In figure 4.13 the intensity of the Balmer lines and the three new peaks are plotted. The behavior of the Balmer lines and the new three peaks are exactly opposite during the change of color. Because the new peaks have a narrow bandwidth, typically for atomic transitions, it seems that during the color change there is some other gas or gasses that produce three spectral lines in the ultraviolet. If another gas enters the lamp this may explain why the Balmer lines loose intensity. This effect is from experience more common when measured with a F-type lamp and less common for a T-type lamp. This could be a possible effect of turbulence in the lamp.

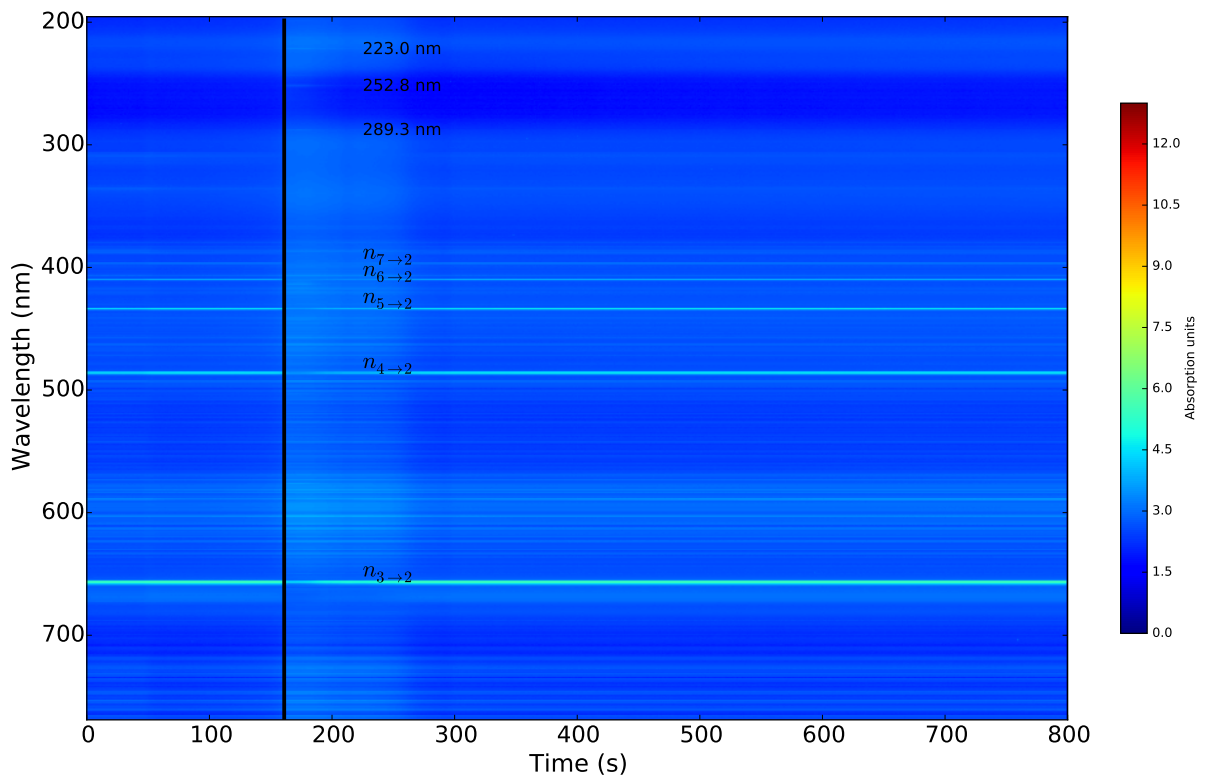


Figure 4.12: 3D spectrum with the intensity of all the wavelengths over the time. The vertical line indicates the point where the color of the lamp changed.

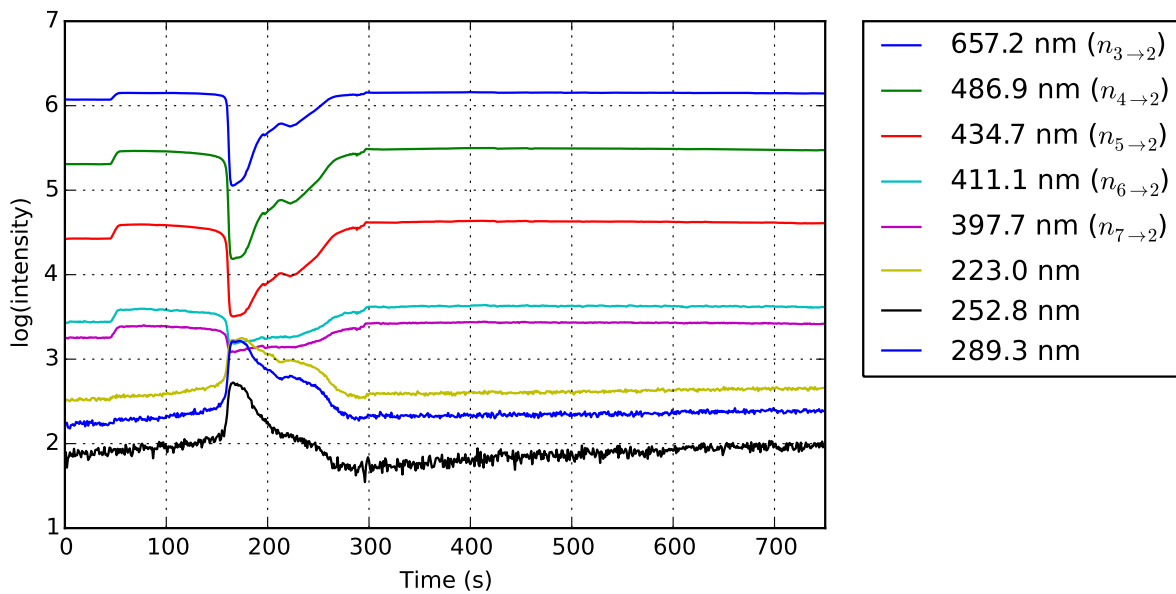


Figure 4.13: Intensity of the Balmer lines and the new lines that appear during the color change.

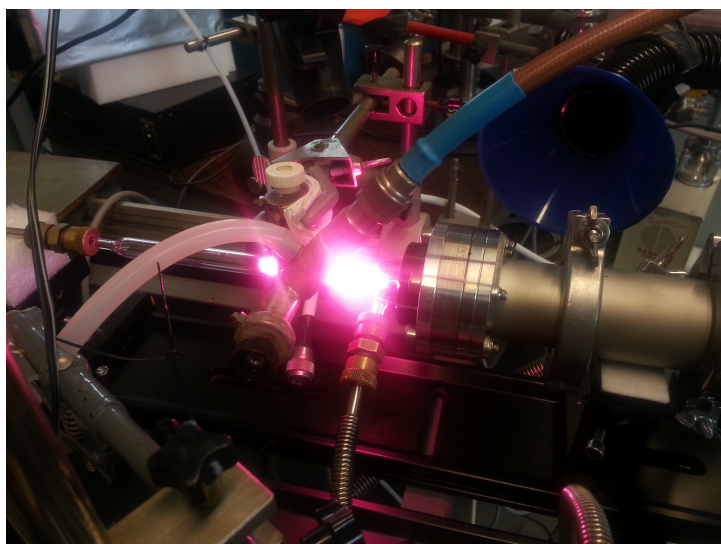


Figure 4.14: The MDHL with normal color.

If this effect shows up during the photodesorption, photodestruction and photochemistry experiments, it could affect the results of the experiments. When the lamp has changed color during the experiment it is possible to see the resulting effect in the mass spectrum. During the experiment there is a continuum background of particles in the main chamber. When the lamp is turned on the background signal will be higher, because the high intensity photons cause the release of the adsorbed species in the walls. The mass spectrum signal increases when the lamp is turned on, after which it stabilizes. When the lamp is turned off the mass spectrum signal will decrease to the original background level. If the intensity of the light increases when changing color, this will also be visible in the mass spectrum.

# Chapter 5

## Conclusion

The results of the measurements with the vacuum ultraviolet spectrometer show that the ratio between the Lyman- $\alpha$  and the molecular part can change over time. During irradiation the Lyman- $\alpha$  peak decreases and the decrease is the biggest after cleaning the window. Measurements have been performed to test what effect the window could have on the spectrum. Probably during the irradiation a layer of dirt forms on both sides of the window. The dirt is not formed without the irradiation, so the energy of the radiation is used to form the dirt. Also it is found that shortly after cleaning the window a constituent absorbs the molecular part. To avoid this, it is advised to pump the lamp and the spectrometer for a while before measuring. Over the last few decades this effect has been neglected in many studies where a MDHL is used. The decreases of the flux have been mentioned, but the present experiments show that the decrease is also wavelength dependent.

The flux of the MDHL is measured by O<sub>2</sub>-actinometry for three different lamp settings and lies in the order of  $10^{13}$  photons s<sup>-1</sup> cm<sup>-2</sup>. Ligterink et al. (2015 in prep.) discuss the spectra and absolute photon fluxes of the three different settings of the MDHL that also have been used here for the actinometry measurements. The only difference between these settings is the type of lamp and the distance from the lamp to the detection techniques. By normalizing the flux and the molecular part of the spectrum the data can be compared with each other. Cruz-Diaz et al. (2014) did already show that the absorption cross section of O<sub>2</sub> ice is lower for Lyman- $\alpha$  than for the molecular part of the spectrum. The experiments discussed in this research thesis show a similar result. Higher Lyman- $\alpha$  flux gives a lower total VUV flux than settings with a high molecular flux. The wavelength dependence of O<sub>2</sub>-actinometry has a big effect on the flux and is therefore not a good manner to measure the absolute photon flux. However this is still a good method to get an idea of the order of magnitude of the flux of a MDHL.

To further investigate the characteristics of the MDHL lamp another set of independent measurements has been performed. The intensity of the Lyman- $\alpha$  peak is determined on the basis of the intensity of the Balmer lines. Three measurements were done at different pressures: 0.4 mbar, 0.8 mbar and 1.2 mbar hydrogen in the MDHL. The calculated Lyman- $\alpha$  fluxes are of the order of  $10^{12}$  photons s<sup>-1</sup> at a distance of about one meter from the lamp and without the correction of the absorption of the MgF<sub>2</sub> window. The intensity of the Lyman- $\alpha$  peak decreases with an increase of the pressure, in agreement with Ligterink et al. (2015 in prep.). Clearly, the experiments presented here give an idea of the involved fluxes and their wavelength dependencies, but more experiments are needed for a full characterization. By measuring the Lyman- $\alpha$  and the Balmer lines at the same time, with a UV/VIS and VUV spectrometer, it can be proven if the calculated Lyman- $\alpha$  fluxes are correct. If this is the case, it is a good way to determine the flux of the Lyman- $\alpha$  peak at a setup with only a spectrometer in the visible range.



# Acknowledgements

Already 17 weeks past by, time flies. I have worked here with great pleasure and I have learned a lot. This internship convinced me to go get a Master's degree. I want to thank everybody of the Sackler group for the nice time I had here and I want to thank a few people in particular. Harold Linnartz for giving me the opportunity to do an internship here and for your supervising. Niels Ligterink for the daily supervision, you always answered my questions enthusiastically even if there were a lot. I have learned a lot from you, dankjewel! Gustavo Cruz Diaz for helping me with the experiments. Vincent Kofman for working on the UV/VIS measurements with me and helping me with Python. Martijn Witlox for fixing things, and Bas Zoutendijk for helping me with LaTeX.



# Bibliography

- V. B. Berestetskii, E. M. Lifshitz, and L. P. Pitaevskii. Quantum electrodynamics.
- Y.-J. Chen, K.-J. Chuang, G. M. Muñoz Caro, M. Nuevo, C.-C. Chu, T.-S. Yih, W.-H. Ip, and C.-Y. R. Wu. Vacuum Ultraviolet Emission Spectrum Measurement of a Microwave-discharge Hydrogen-flow Lamp in Several Configurations: Application to Photodesorption of CO Ice. *ApJ*, 781:15, Jan. 2014. doi: 10.1088/0004-637X/781/1/15.
- H. Cottin, M. H. Moore, and Y. Bénilan. Photodestruction of Relevant Interstellar Molecules in Ice Mixtures. *ApJ*, 590:874–881, June 2003. doi: 10.1086/375149.
- G. A. Cruz-Diaz, G. M. Muñoz Caro, Y.-J. Chen, and T.-S. Yih. Vacuum-UV spectroscopy of interstellar ice analogs. II. Absorption cross-sections of nonpolar ice molecules. *A&A*, 562: A120, Feb. 2014. doi: 10.1051/0004-6361/201322621.
- E. Dartois, O. Marco, G. M. Muñoz-Caro, K. Brooks, D. Deboffe, and L. d’Hendecourt. Organic matter in Seyfert 2 nuclei: Comparison with our Galactic center lines of sight. *A&A*, 423:549–558, Aug. 2004. doi: 10.1051/0004-6361:20047067.
- E. C. Fayolle, M. Bertin, C. Romanzin, X. Michaut, K. I. Öberg, H. Linnartz, and J.-H. Fillion. CO Ice Photodesorption: A Wavelength-dependent Study. *ApJ*, 739:L36, Oct. 2011. doi: 10.1088/2041-8205/739/2/L36.
- E. Herbst and E. F. van Dishoeck. Complex Organic Interstellar Molecules. *ARA&A*, 47: 427–480, Sept. 2009. doi: 10.1146/annurev-astro-082708-101654.
- M. Hogerheijde. *The molecular environment of low-mass protostars*. PhD thesis, Department of Astronomy, University of California, Campbell Hall, Berkeley, CA 94720, USA <EMAIL>michiel@strw.leidenuniv.nl, 1998.
- P. M. Karnarev and D. A. Normov. Energy Balance of Fusion Processes of the Ozone Molecule.
- N. F. W. Ligterink, D. M. Paardekooper, K. J. Chuang, M. L. Both, G. A. Cruz-Diaz, J. H. van Helden, and H. Linnartz. Controlling the Emission Profile of a MW driven H<sub>2</sub> Discharge Lamp to simulate Interstellar Radiation Fields. 2015 in prep.
- G. M. Muñoz Caro, A. Jiménez-Escobar, J. Á. Martín-Gago, C. Rogero, C. Atienza, S. Puertas, J. M. Sobrado, and J. Torres-Redondo. New results on thermal and photodesorption of CO ice using the novel InterStellar Astrochemistry Chamber (ISAC). *A&A*, 522:A108, Nov. 2010. doi: 10.1051/0004-6361/200912462.
- F. H. Shu, F. C. Adams, and S. Lizano. Star formation in molecular clouds - Observation and theory. *ARA&A*, 25:23–81, 1987. doi: 10.1146/annurev.aa.25.090187.000323.



# Appendix A

## Fluxes of other O<sub>2</sub>-actinometry measurements

Actinometry measurements at different settings have been done. In tabel A.1 the settings and corresponding photon flux are displayed. Measurement 5, 6 and 10, in red, are the measurements that have been discussed in section 4.2. The pressure in the main chamber changes from UHV to (U)HV between measurement 6 and 7 because the main turbo pump broke down. Both the F- and T-type lamps have been used in measurements. After measurement 3 a collimating tube is placed in the main chamber. Two different ways of deposition are used, due to a problem with a bend deposition line resulting in the deposition line being misaligned from the window. For all the experiments an ice of 500 ML is grown, except for the last two measurements, where an ice of 2500 ML is grown. After measurement 8 it turned out that a thicker ice was better because of the higher pressure in the main chamber. The oxygen used for the experiments differs between <sup>16</sup>O<sub>2</sub> and <sup>18</sup>O<sub>2</sub>. With <sup>18</sup>O<sub>2</sub> background gas pollution by regular O<sub>2</sub> can be excluded. The sample can be rotated in the main chamber, Appendix B. The experiments are preformed in different ways. At the first two measurements the sample is rotated from 90 degrees to 225 degrees while the lamp remains operational. Here the initial assumption is that during the rotation and measurement with the FTIR the heat shield blocks the irradiation. The fluxes of these two measurements are different. The only difference between the measurements is the speed of turning, so that could mean that the assumption of the heat shield blocking the irradiation when starting the rotation is not correct. At the third measurement the sample gets irradiated at 225 degrees, subsequently the lamp is turned off and the sample is rotated to 270 degrees for the FTIR spectrum. This manner seems more stable. At the seventh measurement the ice did get irradiated under an angle of 45 degrees. When the beam is collimated the flux per cm<sup>-2</sup> will decrease by a factor  $\sqrt{2}$ . This was however not the case. Using this method, more parameters like the position of the FTIR bundle on the ice and the part that is been cut by the cold finger and heat shield have to be known.

Table A.1: Settings with the fluxes of the different  $O_2$ -actinometry measurements. With: UHV= $\sim 10^{-11}$  mbar, (U)HV= $\sim 10^{-9}$  mbar,  $H_2$ =hydrogen, He/ $H_2$ =helium hydrogen mix (4:1) and Tube=collimating tube in the main chamber. The measurements in red are the measurements that have been discussed in section 4.2.

Measurement	1	2	3	4	5	6	7	8	9	10
$P_{cham}$ (mbar)	UHV	UHV	UHV	UHV	UHV	UHV	(U)HV	(U)HV	(U)HV	(U)HV
$P_{lamp}$ (mbar)	0.5	0.5	0.5	0.5	0.5	4.0	0.5	1.43	1.43	1.43
Gas	$H_2$	He/ $H_2$	He/ $H_2$	He/ $H_2$						
Type	F-type	F-type	F-type	T-type						
Tube	No	No	No	Yes						
Deposition	background	background	background	direct						
Ice	$^{16}O_2$	$^{16}O_2$	$^{16}O_2$	$^{18}O_2$	$^{18}O_2$	$^{18}O_2$	$^{16}O_2$	$^{16}O_2$	$^{16}O_2$	$^{18}O_2$
$\angle$ IR	90°	90°	270°	90°	270°	270°	270°	270°	270°	270°
$\angle$ UV	225°	225°	225°	225°	225°	225°	270°	225°	225°	225°
Lamp	On	On	On/Off	On	On/Off	On/Off	On	On/Off	On/Off	On/Off
$\phi$ (pho s $^{-1}$ cm $^{-2}$ )	3.53·10 $^{13}$	5.78·10 $^{13}$	3.86·10 $^{13}$	2.79·10 $^{13}$	3.59·10 $^{13}$	3.39·10 $^{13}$	1.29·10 $^{13}$	4.26·10 $^{13}$	4.38·10 $^{13}$	1.23·10 $^{13}$

# Appendix B

## Position sample

The sample in the CRYOPAD 2 set up can be rotated to make use of different devices that are attached on the main chamber. In figure B.1 a schematic view of the main chamber is shown. The cold finger is placed in the middle of the main chamber. The  $\text{MgF}_2$  transmission window is attached on the cold finger. The degrees are the positions when the flat side of the sample is facing in that specific directions. The beam of the FTIR travels through the chamber from the left to the right. Because use is made of a transmission window, the ice can be measured at two different positions, 90 degrees and 270 degrees. The beam of the FTIR is aligned for the position at 270 degree. When

the sample is placed at 90 degrees, the absorbance of ice can be still measured, but the intensity of the total signal will be lower. For the deposition the sample must be positioned at 135 degrees. To get a maximum signal with the QMS the sample must be placed at 180 degrees and for the UV irradiation the sample must be positioned at 225 degrees.

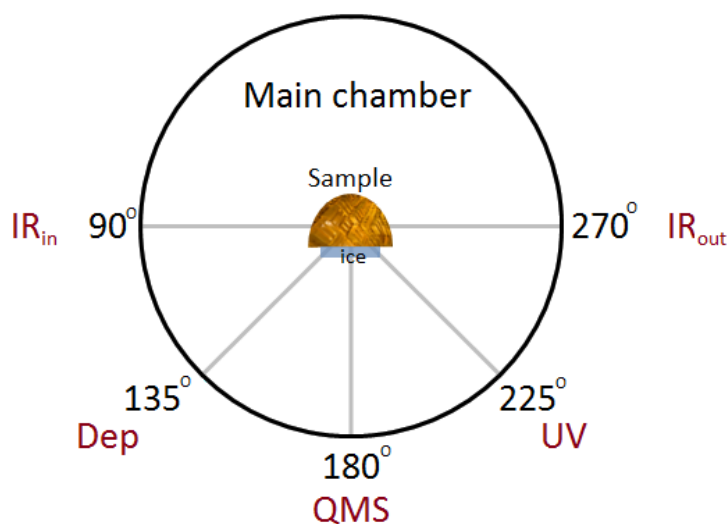


Figure B.1: Position of the sample for the different techniques.



# Appendix C

## Originele omschrijving afstudeeropdracht

Complexe organische moleculen, zg. COMs, ontstaan in de ruimte door oppervlakte reacties op ijzige stofdeeltjes. Daarbij treden UV fotonen (120-160 nm) op als externe trigger. In het laboratorium wordt dit UV licht gesimuleerd met plasma in waterstoflampen dat middels een microgolfontlading wordt gegenereerd.

Een precieze en absolute calibratie van deze lampen is noodzakelijk om lichtgeïnduceerde processen goed te karakteriseren. Deze omvatten fotodesorptie, fotodissociatie en fotochemie.

In het laboratorium voor astrofysica van de Sterrewacht Leiden bevindt zich een opstelling waarmee de wisselwerking van hard UV licht met interstellair ijs kan worden gemeten. Deze opstelling is recentelijk geheel vernieuwd. Temperaturen van  $-260^{\circ}\text{C}$  zijn mogelijk, bij drukken beter dan  $10^{-10}$  mbar. Interstellair ijs wordt met monolaag precisie gededuceerd op een substraat. Voor metingen aan het ijs worden zowel spectroscopische als massa spectrometrische methodes gebruikt.

Het doel van de stage van Miriam Both is om voor verschillende omstandigheden (druk, MW vermogen, gas mengsel, afstand, etc.) de absolute UV fotonen dichtheid van de  $\text{H}_2$  MW lamp te bepalen, zodat op een kwantitatieve manier ter hoogte van het interstellaire ijs analoog fysische/chemische processen bepaald worden als functie van het aantal voorhanden zijnde fotonen. Dit is geen eenvoudige opdracht. De processen zijn golfengete afhankelijk en in het vacuüm UV zijn calibratie metingen zeker niet triviaal. Om dit te realiseren zal een kleine vacuüm opstelling moeten worden gebouwd waarin een (dure) VUV gecalibreerde fotodiode wordt gemonteerd, die als uitgangspunt dient om (minder dure niet gecalibreerde) fotodiodes als referentie geschikt te maken.

Tijdens de stage, zal Miriam Both leren met vacuüm technologie om te gaan, met een plasma lamp, met vacuüm UV licht en calibratie methodes. De stage moet geplaatst worden in de context van het grotere experiment; wat is interstellaire (vaste stof) astrochemie, waarom speelt ijs zo'n belangrijke rol, welke processen vinden plaats, hoe leidt dat tot de vorming van COMs? Het antwoord op deze vragen wordt duidelijk tijdens de stage.

Miriam Both gaat samenwerken met twee SLA medewerkers; MSc. Niels Ligterink en Dr. Gustavo Cruz Diaz. Voertaal zal zowel Nederlands als Engels zijn. Onderdeel van de stage is een veiligheidstraining. Verder zal Miriam Both deelnemen aan colloquia die voor haar onderzoek relevant zijn. Indien gewenst, bestaat ook de mogelijkheid om te participeren in lopende colleges.

Prof. dr. H.V.J. Linnartz